TiO_2 Nanotubes for Drug Delivery and Vascular Tissue Engineering

by

Lily Peng

DISSERTATION

Submitted in partial satisfaction of the requirement for the degree of

DOCTOR OF PHILOSOPHY

in

BIOENGINEERING

in the

GRADUATE DIVISIONS

of the

UNIVERSITY OF CALIFORNIA - SAN FRANCISCO

AND

UNIVERSITY OF CALIFORNIA - BERKELEY

[redacted]

ACKNOWLEDGEMENTS

To my advisor, Tejal Desai, thank you for being so supportive of my interests both within and outside of research.

To Rahul Thakar and Kristy Ainslie, thank you for your insight and advice, scientific and otherwise.

To the Desai Lab, you have made my time in lab strange, enlightening, and entertaining.

To my qualification and dissertation committee members, thank you for your suggestions and help with this dissertation.

To my family, thank you for your encouragement and support.

To my husband, Gavin, you rock.

Funding for this work was provided by the Sandler Family Foundation, Sandler Asthma Basic Research (SABRE) Center Functional Genomics Core Facility and NIH/NCRR UCSF-CTSI Grant (#UL1 RR024131), the National Science Foundation (NSEC), the UCSF MSTP training grant (NIH-NIGMS MSTP #T32GMO7618), and the UCSF Dean's Health Science Fellowship. Immunofluorescence images for this study were

acquired at the Nikon Imaging Center at UCSF. All SEM was performed at the Stanford Nanocharacterization Laboratory through the Stanford CIS Grant Program. Microarrays were performed at the UCSF Shared Microarray Core Facility.

The text of this dissertation is a reprint of the material as it appears in the following papers:

Peng L, Barczak AJ, Barbeau RA, Xiao Y, LaTempa TJ, Grimes CA, and Desai TA. Whole genome expression analysis reveals differential effects of TiO2 nanotubes on vascular cells. *Nano Lett* 10: 143-148, 2010

Peng L, Mendelsohn AD, Latempa TJ, Yoriya S, Grimes CA, and Desai TA. Long-Term Small Molecule and Protein Elution from TiO(2) Nanotubes. *Nano Lett*, 2009.

Peng L, Eltgroth ML, LaTempa TJ, Grimes CA, and Desai TA. The effect of TiO2 nanotubes on endothelial function and smooth muscle proliferation. *Biomaterials* 30: 1268-1272, 2009.

Abstract

The purpose of this project is to investigate how TiO_2 nanotube arrays interact with small molecules, proteins, and cells for local drug delivery and vascular applications. In this first part of this project, TiO_2 nanotubes of various dimensions were used to elute albumin, a large protein molecule, as well as sirolimus and paclitaxel, common small molecule drugs. The nanotubes controlled small molecule diffusion for weeks and large molecule diffusion for a month. Drug eluted from the nanotubes was bioactive and decreased cell proliferation *in vitro*. Elution kinetics was most profoundly affected by tube height. This study demonstrates that TiO_2 nanotubes may be a promising candidate for a drug-eluting implant coating.

To investigate the effects of nanotubular titanium oxide (TiO_2) surface on vascular cells, endothelial (EC) and vascular smooth muscle cells (VSMCs) were cultured on TiO_2 nanotube arrays. Vascular cell response to nanotubes was investigated through immunofluorescence staining, scanning electron microscopy, 5-ethynyl-2′-deoxyuridine proliferation assays, and prostaglandin I_2 (PGI_2) enzyme immunoassays. We found that the nanotubular surface significantly enhances EC proliferation and secretion of PGI_2. The surface also results in a decrease in VSMC proliferation and increased expression of smooth muscle α-actin. These data suggest that engineered nanotopographical cues may influence both EC and VSMC behavior in a manner that may be useful for stent or other vascular applications.

To investigate this further, the response of primary human endothelial (ECs) and vascular smooth muscle cells (VSMCs) to TiO_2 nanotube arrays is studied through gene expression analysis. Microarrays revealed that nanotubes enhanced EC proliferation and motility, decreased VSMC proliferation, and decreased expression of molecules involved in inflammation and coagulation in both cell types. Networks generated from significantly affected genes suggest that cells may be sensing nanotopographical cues via pathways previously implicated in sensing shear stress.

Table of Contents

List of Tables and Figures

Figure 4.1: Nanotube effects on cellular functions and processes of ECs. List of significantly affected cellular functions identified by Ingenuity Pathway Analysis with $p<0.005$ **(A).** Identified functions are sorted into processes relevant to vascular device performance. Genes whose expression is significantly affected by nanotube arrays are plotted according to their likely effects on the four processes **(B)**. Genes that promote a process are represented by open circles (o) with their y-axis on the left, while genes that inhibit a process are represented by filled-in circles (•) and have their y-axis on the right. Plotted this way, genes whose expression pattern is likely to promote a specific process (e.g. enhanced expression of a promoter of proliferation or reduced expression of a gene that inhibits proliferation) will appear on the top half of the graph, and those who would likely inhibit the process would appear on the bottom. Numbers at the top and bottom denote the number of genes that appear on the top or bottom region of the graph. For example, there are 15 EC genes whose expression pattern is consistent with a proliferative phenotype.

Figure 4.2: Top network of genes in ECs whose expression are significantly affected by exposure to nanotube arrays. Red indicates upregulation, green indicates downregulation. Intensity of color is proportional to magnitude of change. For the sake of simplicity, relationships between genes without a significant change in expression are not shown. See original network map in supplemental section, Figure S2.

Figure 4.3: Average expression levels of follistatin (FST), activating transcription factor 3 (ATF3), and early growth response 1 (EGR1) in ECs grown at low densities measured by quantitative PCR. Data is normalized by expression levels of each gene by ECs on flat surfaces and presented as average ± standard deviation. * $p<0.05$ when compared to flat controls, n=3.

Figure 4.4: Nanotube effects on cellular functions and processes of VSMCs. **(A)** List of significantly affected cellular functions identified by Ingenuity Pathway Analysis with $p<0.005$. Identified functions are sorted into processes relevant to vascular device performance. Genes whose expression is significantly affected by nanotube arrays are plotted according to their likely effects on the four processes **(B**), see figure 1 for more detailed explanation. Numbers at the top and bottom denote the number of genes that appear on the top or bottom region of the graph. For example, there are 33 genes whose expression patterns is consistent with a less proliferative phenotype.

Figure 4.5: Top network of genes in VSMCs whose expression are significantly affected by exposure to nanotube arrays. Red indicates upregulation, green indicates downregulation. Intensity of color is proportional to magnitude of change. For the sake of simplicity, relationships between genes without a significant change in expression are not shown. See original network map in supplemental section, Figure S3.

CHAPTER 1: Introduction

There are two main questions that are central in the study of the interactions between biological systems and nanotopograhical materials: (1) how do small molecules, proteins, and cells interact with nanoscale materials? And (2) how do we translate our knowledge about these interactions to clinical applications? This dissertation attempts to answer these questions in two parts. The first section (Chapter 2) focuses on the interaction between TiO_2 nanotubes and small molecules or proteins in the context of a drug eluting surface for local drug delivery. The second part (Chapters 3 and 4) examines how these nanotopographical materials may affect cellular behavior in the context of vascular device or stent applications.

Most eukaryotic cells range from 10-30 μm. Protein components of the cell, such as receptors or scaffolding proteins, are on the order of a few nanometers. Because of this, most protein-protein or protein-small molecule interactions occur on the nanoscale. Recent advances in fabrication techniques allows for the creation of materials with precisely defined nano-features. This enables the examination of how small molecules, proteins, and cells might respond to patterns of varying size, shape, and regularity on a surface with nanotopographical features. This work attempts to examine just one particular type of nanoscale material—TiO_2 nanotube arrays. However, the lessons learned and the questions generated with this model system will likely be applicable to other materials. Thus, we hope this work will contribute to a larger understanding of how cells interact with nanoscale materials and how these interactions can be manipulated for clinical applications.

CHAPTER 2: TiO_2 nanotube surfaces for drug elution

BACKGROUND

Most medical implants procedures such as hip replacements, dental implants, or vascular stents require subsequent drug-therapy regiments to prevent infection, control clotting, or decrease inflammation. Current routes of drug administration, such as oral or intravenous, distribute drugs throughout the body, even though, in many cases, they are only needed at the implant site. Delivery of drugs locally from an implant surface rather than systemically can reduce unnecessary side effects as well as the amount of drug required to reach the same efficacy. A common strategy to allow drug elution from an implant surface involves the application of a drug-loaded polymer coating. For example, in drug-eluting stents (DES) a bare metal stent is coated in a polymer that slowly releases drugs such as sirolimus or paclitaxel to limit cell proliferation and restenosis. While effective in delivering drug for several weeks, the polymer degradation may induce an inflammatory response, activating phagocytes and increasing vascular smooth muscle proliferation,[1] which can lead to implant failure. To address these problems, the newest developments in drug eluting surfaces are focused upon non-polymer based drug delivery platforms, such as surfaces covered with an inorganic oxide, such as Al_2O_3 (alumina),[2] or sandblasted to give the implant a nanoporous or microporous topography.[3] These surfaces are capable of eluting drugs for months and, when used to modify stents, are effective in reducing intimal hyperplasia in animals and humans. Despite their successes, additional studies have shown that both alumina and sandblasted stainless steel can also provoke an inflammatory response.[4,5]

A more suitable candidate for a drug-eluting implant coating is titanium dioxide (TiO_2). Titianium dioxide is an inert material that spontaneously forms on titanium implants, making the implants extremely biocompatible. Bulk TiO_2 has been shown to have good hemocompatibility as TiO_2 coatings have been shown reduce clotting and platelet activation on nickel-titanium surgical alloys.[6] Furthermore, highly ordered nanotubular arrays with tube diameters that range from 22 – 300 nm[7] and lengths of up to 1 mm[8, 9] can be easily fabricated through a simple electrochemical process on titanium foil. Diameters of these tubes is determined by applied anodization voltage, and the length is controlled by electrolyte composition and duration of anodization.[10] TiO_2 nanotubes have shown promise in a variety of biological applications, exhibiting low immunogenicity,[11] a capacity to direct stem cell fate,[12] and promote function in osteoblasts.[13] In addition, previous studies suggest that they may be able to control protein[14] or antibiotic release[15] on the order of hours. However, it was unclear in these studies that drug elution was due to the surface's nanostructure. Since these studies did not include a consistent and reliable method of removing drug that was not within the tubes, the observed elution curves were likely significantly impacted by a surface layer of drug. Furthermore, to be clinically useful, drug elution from these implants would ideally last for a longer period of time, on the order of days or weeks.

METHODS

TiO_2 nanotube fabrication. TiO_2 nanotube arrays were formed via anodic oxidation in an electrolytic solution containing 0.2M Sodium Citrate Tribasic, 1M Sodium Hydrogen Sulfate, and 0.1M Potassium Fluoride, with Sodium Hydroxide added to adjust

the pH of the solution. Titanium foil (0.25mm thick, 99.7% purity, Alfa Aesar) were anodized at a constant DC potential for 17 hours in a two-electrode electrochemical cell with a platinum foil as the counter electrode. The average length and pore diameter of the nanotubes were scaled by varying the pH of the electrolyte and the DC potential during anodization. Nanotubes 1 μm in length with an average pore diameter of 100 nm were prepared by anodization using 20 V bias in the 2 pH electrolyte. The 100 nm diameter 5 μm long tubes were prepared using a 25V bias in a 5pH bath.

Samples were subsequently annealed at a temperature of 500 °C for the 1μm in oxygen ambient to crystallize the nanotubes. Heating and cooling rates of 1 °C/min were used with a dwell time of 6 hours. Surfaces were sterilized with 70% ethanol and UV prior to use in tissue culture.

Drug loading. 0.5 cm x 0.5 cm TiO_2 nanotube and control flat pieces were rinsed with dH_2O, 70% ethanol, and allowed to air dry. Sirolimus (Calbiochem, San Diego, CA), Oregon-green conjugated paclitaxel (Invitrogen, Carlsbad, CA), and FITC-BSA were diluted in methanol, DMSO, and ddH_2O respectively. Some of the nanotube arrays were treated with oxygen-plasma for 60 seconds prior to drug loading. 1 μl of concentrated sirolimus (5 mg/ml), paclitaxel (1 μg/ml), or BSA (10 mg/ml) was applied to each surface. Samples were allowed to air dry in a chemical hood. After drying, the loading procedure was repeated two additional times for sirolimus, three for BSA, and four for paclitaxel.

The loaded pieces were placed on a spin-coater (Specialty Coating Systems, Indianapolis, IN) and rotated at >1000 rpm while 200 μl of solvent (methanol for

paclitaxel and sirolimus, 70% ethanol for BSA) was added to the samples to remove the surface layer of drug.

The samples were immersed in 500 µl of PBS in at 37 °C in capped eppendorf tubes. The tubes were then agitated on an orbital shaker at approximately 100 rpm to eliminate boundary layers. Samples were taken at specified intervals by removing the entire volume of PBS and replacing with fresh PBS each time. Paclitaxel and BSA samples were measured with a fluorometer (Packard Instrument Company, Downer Hills, IL) while sirolimus concentrations were measured using a UV-plate reader (Molecular Devices, Sunnyvale, CA).

MOVAS cell culture. Mouse aortic vascular smooth muscle cells (ATCC, Manassas, VA) were cultured according to the manufacturer's instructions. The cells were grown in high glucose (4.5 g/L) DMEM with 10% FBS, 0.2 mg/ml G418, 4 mM L-glutamine, and 1.5 g/L sodium bicarbonate. The cells were cultured in a humidified 95% air/5% CO_2 incubator at 37°C. Cells used in this experiment were passaged less than ten times after being obtained from the facility.

Drug elution and vascular smooth muscle cell proliferation. Mouse vascular smooth muscle cells (MOVAS) were obtained from American Type Culture Collection (Manassas, VA) and cultured according to ATCC instructions. The cells were seeded at 5000 cells/cm^2 in 12-well plates with 1.5 ml of media. TiO_2 nanotube and flat surfaces loaded with sirolimus were placed into transwells and put into the wells with the cells. TiO_2 loaded with methanol and blank transwell inserts also served as controls. After two days, the cells were trypsinized and counted with a hemacytometer. The transwells and

pieces were transferred to a fresh plate of cells at the same original seeding density. Cell counts were then measured in another two days and the procedure was repeated for 10 days. The doubling times and growth rates were calculated from the cell number and normalized by that of the blank transwell controls.

Mathematic modeling of drug elution. The experimentally-obtained data indicates that there is first a rapid elution phase of the molecules from the TiO_2 nanotubular surface followed by a slower elution phase. In order to model this behavior and extrapolate from the data how much of the drug underwent rapid vs. slow elution and what the diffusivities associated with each phase were, a two-phase elution model was derived as follows.

Assuming Fickian diffusion, Fick's first law of diffusion as applied to this system describes the chemical flux (J) driven by the concentration gradient ($\Delta C(t)$) across the distance (l) the molecule travels across the concentration gradient as a function of the diffusivity (D) associated with the material properties: $J = -D\frac{\Delta C(t)}{l}$. The chemical flux, J, can be described as the mass gradient ($dM(t)$) across l divided by the area (A) with respect to time (dt): $J = \frac{dM(t)}{A \cdot dt}$. The samples were taken in perfect sink conditions, and therefore for this model we assume that the concentration in the sample reservoir is always zero and the concentration on the TiO_2 is defined as the mass of the molecules on the TiO_2 ($M(t)$) divided by the volume those molecules take up (V): $\Delta C(t) = \frac{M(t)}{V}$. From this we are left with: $\frac{dM(t)}{M(t)} = -\frac{AD}{lV}dt$. Let $\frac{AD}{lV} = C$. Integrating both sides and solving for

$M(t)$ yields the equation $M(t) = M_0 \cdot e^{-Ct}$. For two-phase elution, fast and slow, assuming that the elution phases are independent from each other $M(t) = M_{i,s} \cdot e^{-C_s t} + M_{i,f} \cdot e^{-C_f t}$, where $M_{i,s} + M_{i,f} = M_0$, or the total mass of drug eluted from the TiO_2. By examining each experimentally-determined elution curve it becomes clear that after a certain time point only the slow elution phase is relevant. From this data, C_s can be extracted and $M_{i,s}$ can be extrapolated. Knowing these constants and M_0 which is measured experimentally, one can examine the first couple of data points to determine C_f and $M_{i,f}$. These constants are shown in table 2.1 and a graph demonstrating how closely this model resembles experimentally-obtained results is shown in figure 2.4.

RESULTS AND DISCUSSION

In order to extend the duration of drug elution and better understand how nanotube dimensions may affect elution kinetics, we fabricated a series of arrays with varied lengths and sizes (Figure 2.1). The arrays were then loaded with fluorescently labeled paclitaxel, a 1.3 kDa drug with a small (<0.5 nm) hydrodynamic radius. Clinically, paclitaxel is commonly used as an anti-proliferative agent to treat inflammation, cancer, and stent restenosis. After loading, the surfaces were then rinsed using a rotating spinner to remove the surface layer, immersed in PBS at 37 °C, and agitated to eliminate boundary layers. Drug elution was measured at various time points and for three weeks in perfect sink conditions.

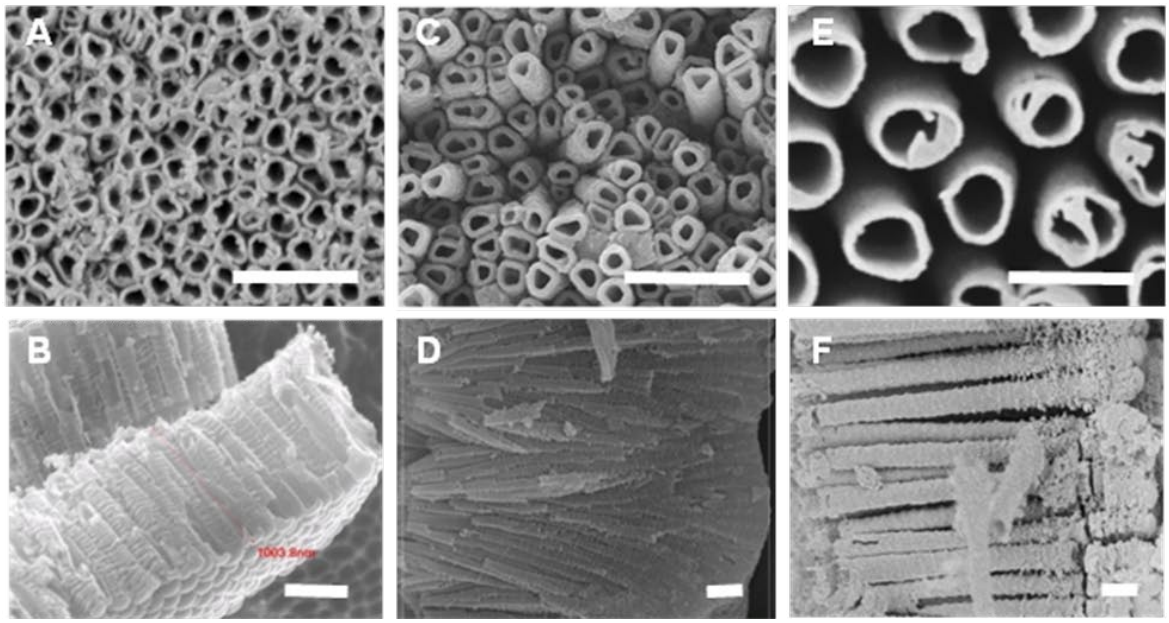

Figure 2.1: SEM images of TiO_2 nanotubes with various dimensions. Each column corresponds to one sample type. First row depicts top view. Bottom row shows side views. Scale bars represent 500 nm. (A, B) d=100 nm, h=1 μm; (C,D) d=100 nm, h=5 μm; (E,F) d=300 nm, h=5 μm.

Maximum drug elution was reached at approximately two weeks, after which the amount of additional drug eluted was negligible. We found that total drug elution was most profoundly affected by nanotube length. Comparison between nanotube arrays with the same diameter (100 nm), but different lengths (1 μm vs. 5 μm) revealed that on average nanotubes 1 μm in length held less than half the amount of drug trapped by 5 μm nanotubes (Figure 2.2A). This increase in drug loading is not unexpected since longer tubes translate to larger volumes available for drug loading. Larger diameter nanotubes eluted less drug than 100 nm nanotubes of the same length (Figure 2.2A). This difference may be due to drug loss during the rinse step as a result of the larger diameter and the lower packing density of the 300 nm tubes. The wider diameter may allow significantly more solvent to enter the nanotubes. In addition, drug that was loaded into the large gaps between the tubes was more likely to be stripped off during the wash step.

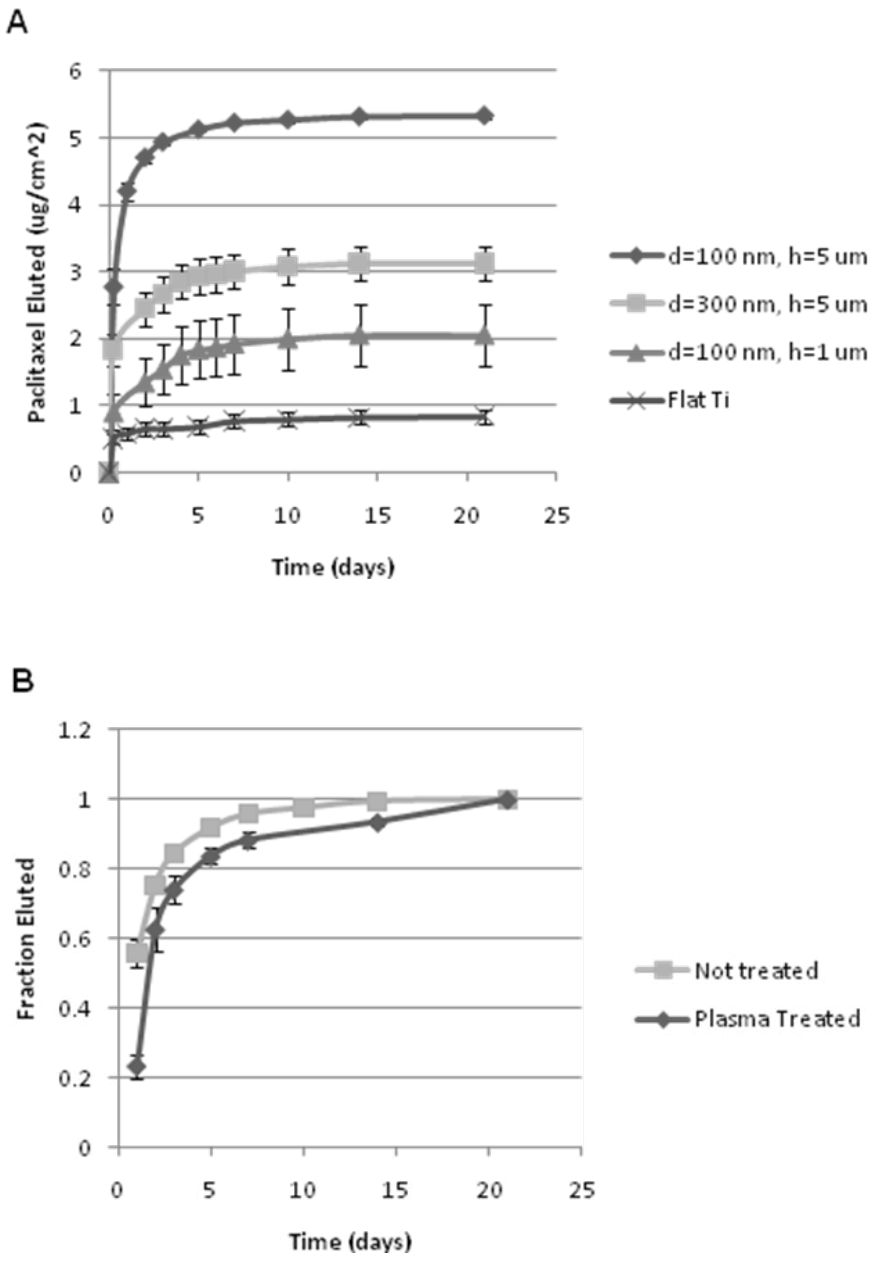

Figure 2.2: (A) Paclitaxel elution for nanotube arrays of various dimensions. (B) Long-term fractional elution of non-treated and plasma treated nanotube arrays 100 nm in diameter and 5 μm in height. Analysis is limited to mass eluted after the first 24 hours. Data is presented as average ± stdev.

Since the 100 nm diameter 5 μm long nanotubes performed significantly better than nanotubes of other dimensions, these samples were chosen for further characterization. It has been previously shown that capillary force dependent filling of non-treated nanotube arrays allows solvents to penetrate less than 1 μm into the tubes, and increasing the

hydrophilicity of the surfaces may enhance the penetration of polar solvents.[16] To test this hypothesis, nanotubes arrays 5 μm in length and 100 nm in diameter were plasma-treated to increase surface hydrophilicity before being loaded with paclitaxel. The surface treatment seemed to decrease the rate of drug elution after 24 hours (Figure 2.2B) but did not seem to significantly improve other aspects of drug elution. Since increased solvent penetration should have translated to increased total drug elution, it is possible that the plasma did not penetrate significantly deeper into the tubes than the solvent did in the untreated samples. It is also possible that non-treated surfaces already were hydrophilic enough that solvents reached the maximum depth attainable by using only capillary-force dependent filling, and that any further improvements would require the application of another filling method.

In addition to paclitaxel, we also measured elution curves of sirolimus, another commonly used small molecule anti-proliferative agent, and bovine serum albumin (BSA), a large globular protein from the 100 nm diameter 5 μm tall nanotubes. Sirolimus, with a molecular weight of 0.91 kDa, is about the same size as paclitaxel. In contrast, BSA, which is about 66 kDa, has a hydrodynamic radius of approximately 2-3 nm. We found that while total mass of drug eluted was similar between the two compounds, sirolimus had a more gradual elution curve than paclitaxel. While nanotubes controlled the elution of small molecules for 7-14 days, they were capable of controlling the delivery of larger molecules like BSA for greater than 30 days (Figure 2.3A). Changes in height and diameter yielded a similar trend in BSA elution and paclitaxel elution. The difference between nanotubes of various dimensions was not significant because of the large variation between samples of the same dimensions (Figure 2.3B).

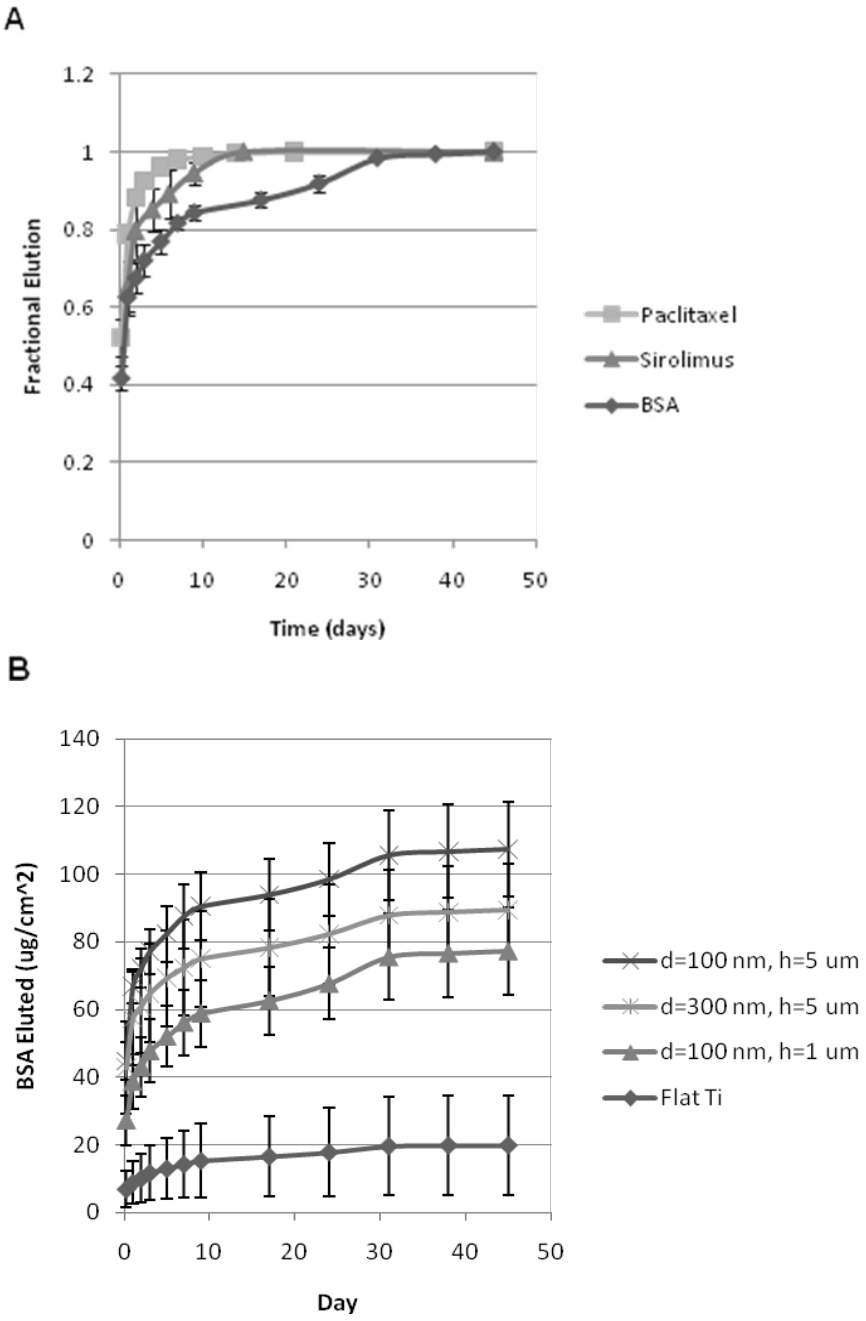

Figure 2.3: (A) Fractional elution of paclitaxel, sirolimus, and BSA. (B) BSA elution of nanotubes with various dimensions. Data is presented as average ± stdev. n=3 for each condition

To further characterize the elution kinetics of the nanotube arrays, fractional elution curves of paclitaxel and BSA were modeled using a derivation of Fick's first law of diffusion. Data fitting and analysis suggests that elution can be described in a two phase elution model, with an initial rapid phase within the first 24 hours and a slower phase thereafter:

$$M(t) = M_{i,f}e^{-C_f t} + M_{i,s}e^{-C_s t} \quad ,$$

In a Fickian diffusion model, $C_f = \frac{D_f}{l_f^2}$, $C_s = \frac{D_s}{l_s^2}$, D_x=Diffusion Constant, $M_{i,x}$=Initial Mass, l_x=distance by which the drug molecule must travel across the concentration gradient with diffusivity D that drives its diffusion, and the *s* and *f* subscripts refer to the slow and fast phases respectively. Mass elution associated with the fast phase generally increased with tube height but decrease with tube diameter, while mass eluted during the slow phase largely remained constant (Table 2.1). C_f also remained roughly constant for most cases, with the highest diffusivity observed for the 300 nm nanotubes, which may be due to the lower density packing of the tubes. There was a slight trend toward increasing C_s with increasing diameter, but it is clear that tube diameter does not have a profound impact on elution kinetics. This is not surprising since zero order diffusion is usually seen with pore dimensions that are on the order of the molecule itself. Since paclitaxel has a radius of <0.5 nm, nanotubes that are 100 nm or greater in diameters too large to allow for single-file diffusion. Nevertheless, molecule type seemed to have the most profound effect on the diffusion constant term, as BSA elution yielded values for C_f and C_s that were 0.75 and 0.20 times of that paclitaxel. Furthermore, the two-phase elution model resembles experimentally-obtained data remarkably well (Figure 2.4).

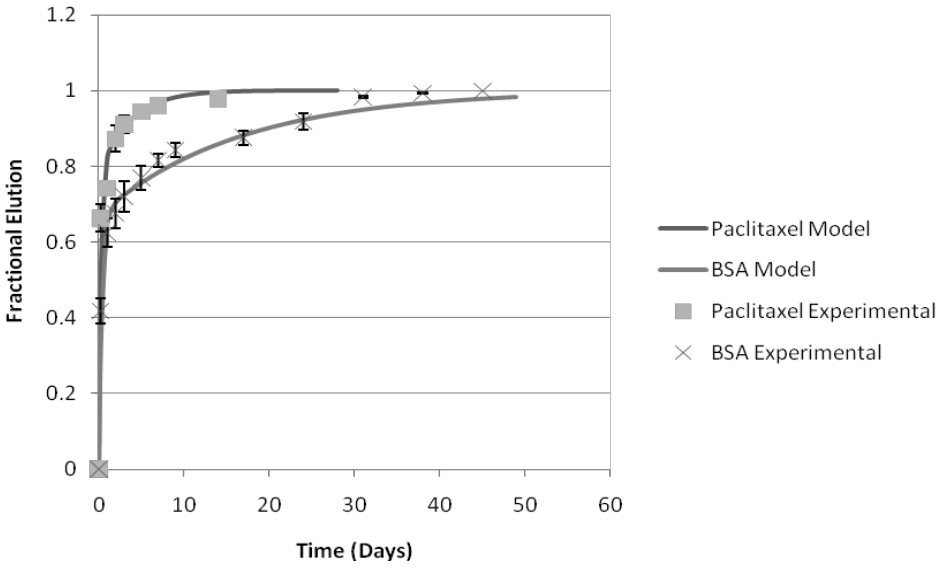

Figure 2.4: Fractional elution of paclitaxel and BSA from nanotubes with 100 nm diameter and 5 μm height, plasma-treated. Both experimental values and curves generated from the constants in table 5 using the two-phase diffusion model are shown. Data is presented as average ± stdev.

Nanotube Dimensions	Drug	Initial Fast Mass	Initial Slow Mass	C_f	C_s	Initial Total Mass
Flat Titanium	Paclitaxel	0.480	0.358	-5.38	-0.2208	0.837
d=100 nm, h=1 um	Paclitaxel	0.93	1.12	-3.92	-0.3058	2.05
d=100 nm, h=5 um	Paclitaxel	4.30	1.03	-3.53	-0.3027	5.33
d=300 nm, h=5 um	Paclitaxel	2.04	1.08	-4.89	-0.3216	3.12
Flat Titanium	BSA	9.24	11.0	-2.70	-0.0903	20.2
d=100 nm, h=1 um	BSA	43.1	36.8	-2.49	-0.0717	80.0
d=100 nm, h=5 um	BSA	70.8	39.2	-2.81	-0.0878	110.
d=300 nm, h=5 um	BSA	61.0	30.4	-3.27	-0.0745	91.5

Table 2.1: Table of constants generated from data-fitting experimental data to the two-phase elution model presented: $M(t) = M_{i,f}e^{-C_f t} + M_{i,s}e^{-C_s t}$

Lastly, nanotube arrays of 100 nm in diameter and 5 μm in length were also used to study the effect of drug elution on vascular smooth muscle cells. Because sirolimus displayed a similar total drug loading capacity but was a more potent drug with slower release kinetics than paclitaxel, it was used to determine if nanotubes were able to control diffusion of small molecules and preserve drug activity *in vitro*. To ensure that any change in cell behavior was due to the drug eluting from the nanotubes only and not in response to the nanotopgraphy, a transwell set up was employed. The top chamber, which held the nanotube samples, and was separated from the bottom chamber, which contained the cells, by a transwell membrane that would allow the diffusion of drug, but ensure that cells do not come in direct contact with the nanotube arrays. Mouse vascular smooth muscle cells were seeded on tissue culture polystyrene surfaces in the bottom chamber. Sirolimus-loaded nanotube pieces were placed into transwell inserts in cell cultures, and the transwell with the nanotube pieces were removed every two days and placed into new cultures of cells. Cells exposed to the nanotubes loaded with solvent only, flat controls, and blanks all showed similar growth rates (Figure 2.5). However, cells exposed to drug-loaded nanotubes exhibited growth rates that were significantly blunted through day 8, confirming that the drug loaded-nanotubes had been delivering active drug over that time period. These data confirmed that the nanotube arrays are amenable to bioactive drug elution and may be viable alternatives to polymer-based drug elution platforms.

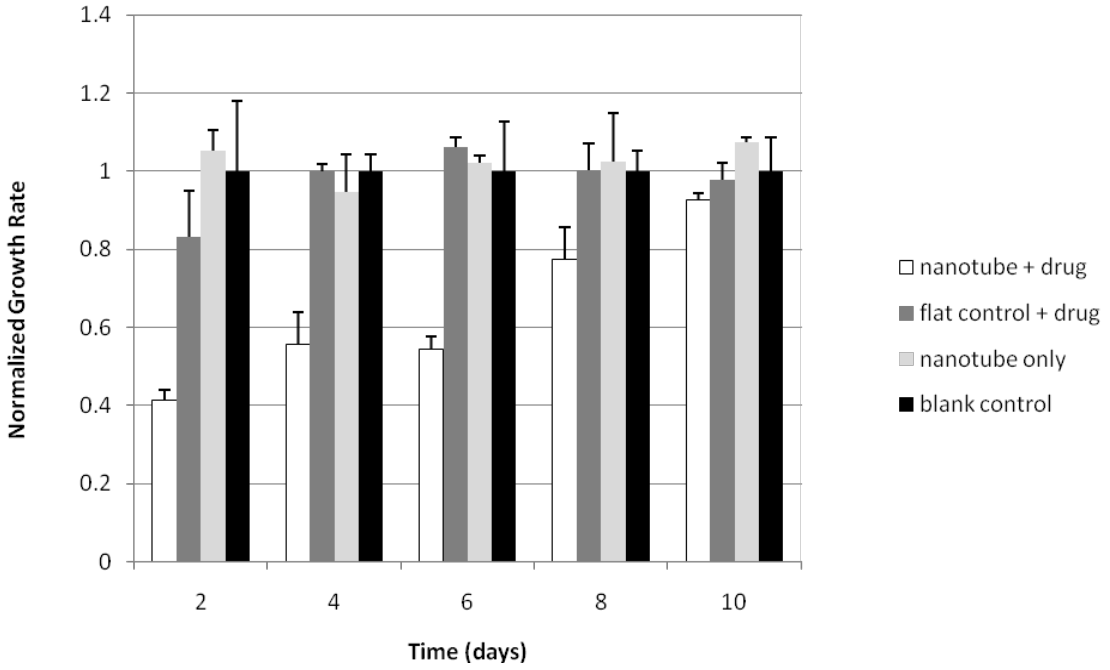

Figure 2.5: The effect of sirolimus loaded nanotubes pieces on the growth rate of vascular smooth muscle cells. Data is presented as average + stdev. *$p<0.05$ vs. Control

This study demonstrated that TiO_2 nanotubes can control small molecule delivery on the order of weeks and larger molecules on the order of months. The changes in drug delivery observed with variations in nanotube dimensions support the hypothesis that the nanotopography of the tubes is directly responsible for the drug elution behavior. We found that at size scales of 100 nm and larger, diffusion of both types of molecules was largely insensitive to tube diameter, but total drug elution was dependent on tube length, with longer tubes performing better than shorter ones. Mathematical modeling of the data showed a two phase elution that can be described by derivations of Fick's first law. *In vitro* studies showed that drug eluted from the surfaces was active and could blunt differentiation for approximately 7 days. This study demonstrated the feasibility of using

TiO_2 nanotubes for long term drug elution. Because the nanotubes used in this study were capable of trapping relatively small amounts of drug, this current system is best suited for delivery of potent molecules. Improvements to increase drug loading capacity, extend elution duration, and linearize drug elution kinetics would greatly increase the clinical applicability of this technology.

CHAPTER 3: TiO_2 nanotubes and vascular cell behavior

BACKGROUND

Coronary artery disease is the leading cause of death in the United States.[17] Severe cases are commonly treated with vascular prostheses such as stents or vascular grafts. However, such interventions are associated with major complications such as narrowing of the prosthesis due to vascular smooth muscle cell (VSMC) proliferation and thrombosis as a result of injury and dysfunction of endothelial cells (EC). Clearly, the modulation of cellular behavior is important in the design of next generation vascular devices.

Nano- and micro-topography can control the behavior of many different types of cells, including ECs and VSMCs, and has been investigated extensively in two-dimensional and, more recently, three-dimensional systems.[18] Studies with ECs suggest that increasing surface roughness may encourage cell proliferation.[19, 20] Rapid re-endothelialization after procedures such as artificial vascular grafts and stent implantation can improve patient outcome by decreasing thrombosis risks and shortening anti-coagulative therapy duration. In addition to preventing thrombogenesis, ECs also promote VSMC differentiation and quiescence. When the EC layer is denuded (e.g. during a stent implantation), VSMCs can lose their differentiated phenotype. In this undifferentiated state, the VSMCs assume a proliferative phenotype and undergo cell division, resulting in intimal hyperplasia.[21] Because intimal hyperplasia is the major cause of restenosis or vessel blockage, there is great interest in targeting VSMCs directly

to prevent stent or graft failure. The direct effect of topography on VSMC proliferation and phenotype has been extensively studied. While random surface topography can promote VSMC proliferation,[20] highly ordered features, such as aligned grooves, can result in VSMC alignment, decreased proliferation, and increased differentiation.[22] Hence, understanding the interactions between ECs, VSMCs, and topography are important aspects in engineering better stents and vascular grafts.

As described in Chapter 2, TiO_2 nanotube arrays are biocompatible surface coatings that can be patterned upon a titanium bulk surface through electrochemical anodization. In addition to demonstrating the possibility of being useful for orthopedic applications, nanotubes may be also be used in vascular applications, enhancing endothelial cell ECM production and motility.[23] Here we investigate the effects of nanotubes on both VSMCs and ECs and show that the surface may be able to address issues associated with re-endothelialization and restenosis.

MATERIALS AND METHODS

TiO_2 nanotube fabrication. TiO_2 nanotube arrays were formed via anodic oxidation in an electrolytic solution containing 0.2M Sodium Citrate Tribasic, 1M Sodium Hydrogen Sulfate, and 0.1M Potassium Fluoride, with Sodium Hydroxide added to adjust the pH of the solution. Titanium foil (0.25mm thick, 99.7% purity, Alfa Aesar) were anodized at a constant DC potential for 17 hours in a two-electrode electrochemical cell with a platinum foil as the counter electrode. The average length and pore diameter of the nanotubes were scaled by varying the pH of the electrolyte and the DC potential

during anodization. Nanotubes 1 μm in length with an average pore diameter of 30 nm were prepared by anodization using 10 V bias in the 4 pH electrolyte. Samples were subsequently annealed at a temperature of 500 °C for the 1μm in oxygen ambient to crystallize the nanotubes. Heating and cooling rates of 1 °C/min were used with a dwell time of 6 hours. Surfaces were sterilized with 70% ethanol and UV prior to use in tissue culture.

BAEC cell culture. Bovine aortic endothelial cells were obtained from the UCSF Cell Culture Facility (San Francisco) and cultured in low glucose (1g/L) Dulbecco's Modified Eagle's Medium (DMEM) with 10% fetal bovine serum (FBS), 100 units/ml penicillin, 100 units/ml streptomycin, and 110 g/L sodium pyruvate. The cells were cultured in a humidified 95% air/5% CO_2 incubator at 37°C. Cells used in this experiment were passaged less than ten times after being obtained from the facility.

MOVAS cell culture. Mouse aortic vascular smooth muscle cells (ATCC, Manassas, VA) were cultured according to the manufacturer's instructions. The cells were grown in high glucose (4.5 g/L) DMEM with 10% FBS, 0.2 mg/ml G418, 4 mM L-glutamine, and 1.5 g/L sodium bicarbonate. The cells were cultured in a humidified 95% air/5% CO_2 incubator at 37°C. Cells used in this experiment were passaged less than ten times after being obtained from the facility.

Immunostaining for actin. VSMCs and ECs were seeded on flat Ti surfaces and nanotubular TiO2 surfaces at a density of 5 X 10^3 cells/cm^2. Cells were incubated in complete media under standard culture conditions. After 24 hours, cells were fixed in 4% paraformaldehyde in PBS. Subsequently, the cells permeabilized with 0.5% Triton X-

100 in PBS, blocked with 1% BSA in PBS for 30 minutes, and stained Alexa Fluor 488 phalloidin (Invitrogen, Carlsbad, CA) for 60 minutes at room temperature. ECs were then counterstained with Hoescht to image the nucleus. Samples were mounted and imaged using a Nikon C1si Spectral Confocal microscope. ImageJ was used to determine cell coverage area.

SEM for cell morphological examination. MOVAS cells were seeded at a density of 5 x 10^3/cm^2 and grown for 24 hours in complete medium on nanotube and flat control surfaces. The surfaces were rinsed with PBS and then soaked in the primary fixative of 3% glutaraldehyde (Sigma, St. Louis, MO), 0.1M of sodium cacodylate (Polysciences, Warrington, PA), and 0.1M sucrose (Sigma) for 45 min. The surfaces were subjected to two 5-min washes with a buffer containing 0.1M sodium cacodylate and 0.1M sucrose. The cells were then dehydrated by replacing the buffer with increasing concentrations of ethanol (35%, 50%, 70%, 95% and 100%) for 10 min each. Further, the cells were dried by replacing ethanol by hexamethyldisilazane (HMDS) (Polysciences) for 10 min. The HMDS was removed, and the surfaces were air dried for 30 min. SEM imaging was conducted on the Sirion Scanning Electron Microscope at 5 kV after the surfaces were sputter coated in gold. The sputter coater was set at current of 20mA and pressure of 0.05 mbar for 20 s to deposit a 10 nm layer of gold.

EdU proliferation assay. For assessment of cell proliferation, BAECs were seeded on flat Ti and TiO_2 nanotube surfaces at a density of 5x10^3 cells per cm^2 culture surface area. Cells were incubated under standard conditions in complete media. At days 1 and 3 after seeding, cell proliferation was detected using incorporation of 5-ethynyl-2'-deoxyuridine (EdU) with the Click-iT EdU Cell Proliferation Assay Kit (Invitrogen).

Briefly, cells were incubated with 10μM EdU for 45 minutes before fixation, permeabilization, and EdU staining, which were carried out according to the kit's protocol. Cell nuclei were stained with Hoechst 33342 (Invitrogen) at a concentration of 5μg/ml for 30 minutes. The proportion of nucleated cells incorporating EdU was determined by fluorescence microscopy.

Western blotting procedure. MOVAS cells were seeded at a density of 5 x 10^4/cm^2 and harvested after 24 hours. Whole-cell lysates were prepared by disruption of the cells with RIPA buffer (20 mM Tris-MOPS [pH 7.4], 150 mM NaCl, 1 mM EDTA, 1 mM EGTA, 1% NP-40) plus 1X protease inhibitor cocktail and 1X phophotase inhibitor for 5 min on ice, centrifugation at 16,000 x *g* to remove insoluble materials, and boiling at 100°C for 5 min. The lysates's protein concentrations were measured using a micro BCA assay (Pierce, Rockford, IL) to ensure equal protein loading. The samples were resolved by 10% NuPAGE gels (Invitrogen) and transferred to polyvinylidene difluoride membranes (Millipore, Billerica, MA). After transfer, the blots were cut at the 40 kDa marker and probed separately for smooth muscle α-actin (42 kDa) and glyceraldehyde 3-phosphate dehydrogenase (GAPDH, 38kDa). Mouse anti-smooth muscle α-actin (Sigma) and mouse anti-GAPDH (Santa Cruz Biotechnology, Santa Cruz, CA) were use as the primary antibodies and goat anti-mouse HRP (Pierce) as the secondary. Antibodies were detected by chemiluminescence (PerkinElmer), Pierce film, and a Konica SRX-101A developer. Intensity of the bands were quantified using ImageJ.

PGI_2 EIA assay. BAECs were seeded at a density of 1 x 10^4 cells/cm^2 and allowed to attach for 24 hours in complete media. The cells where then washed twice with PBS and the media was replaced with phenol-red free DMEM without FBS. After an additional

24 hours, the supernatant was harvested and centrifuged for 10 min to remove cellular debris. The cells remaining on the surfaces were fixed, stained, and counted. PGI_2 secretion in the supernatant was measured using an EIA kit (Cayman Chemicals, Ann Arbor, MI) according to the manufacturer's instructions. The amount of PGI_2 per cell was calculated by dividing the total amount secreted by the number of cells on the surface.

RESULTS AND DISCUSSION

Since rapid re-endothelialization is crucial to the success of a vascular device, it is important to understand how endothelial cells will interact with TiO_2 nanostructured surfaces. To determine how nanotopography affects the morphology of ECs, bovine aortic endothelial cells (BAECs) were grown on nanotubular and flat surfaces. The cells were fixed and stained with phallodin to image the actin cytoskeleton and Hoechst to stain the nucleus. Confocal microscopy (Figure 3.1) revealed that cells on nanotubular substrates had elongated morphologies whereas cells on the flat surfaces were more spread out and cover greater surface areas. Because of the elongation, cells on nanotubes on average covered ~60% of the average area occupied by the control cells. While elongation is seen when ECs are exposed to mechanical forces, such as shear stress or hydrostatic pressure,[24] elongation can also be a response to topographical cues. ECs have been observed to assume a more linear morphology in response to a honeycomb-patterned microtopography, similar in shape but much larger in size as compared to the nanotubes. The elongated cells also had increased proliferation and extracellular matrix production when compared to their spread out counterparts.[25] In addition, elongated cell

have been observed to have higher migrations speeds.[26] Since migration into wound site is a major mode re-endothelialization, enhanced EC motility may greatly improve healing after injury or device implantation.

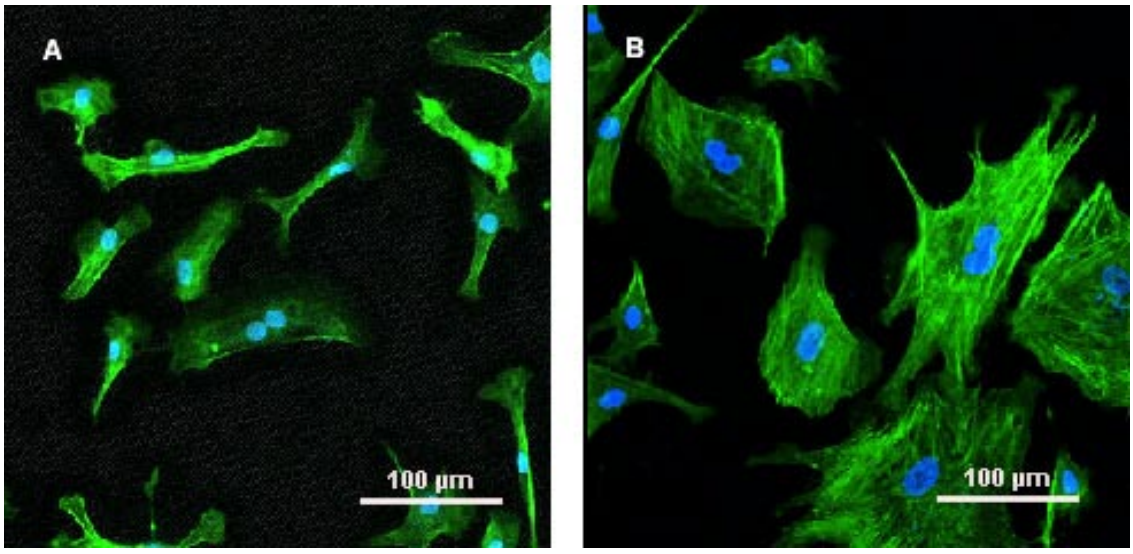

Figure 3.1: F-actin (green) and nuclear (blue) stains of BAEC grown on (A) nanotubular TiO_2 versus (B) flat surfaces for 24 hours.

In addition to EC studies, VSMC morphological response to nanotube arrays was also investigated through immunostaining and scanning electron microscopy (SEM) of mouse vascular smooth muscle cells (MOVASs). F-actin staining revealed cells that were more rounded and clustered on nanotubes than on controls. SEM highlighted a tendency for the VSMCs to adhere to and grow on top of each other rather than the nanotubes. Whereas cells on flat control surfaces sent out numerous long processes to maximize contact with the substrate, cells on the nanotubes had preferred to minimize contact with the nanotube surface. When compared to controls, the size of cells on nanotubes was on average ~40% that of controls (Figure 3.2). This difference in morphology was most striking in the first few days after which cells on nanotubes became increasingly similar

to those on controls, possibly due to extracellular matrix production and cell growth that obscured the nanotopographical features. However, the smaller and more rounded morphology observed initially may indicate that VSMCs are less likely to thrive and proliferate on nanotubes.

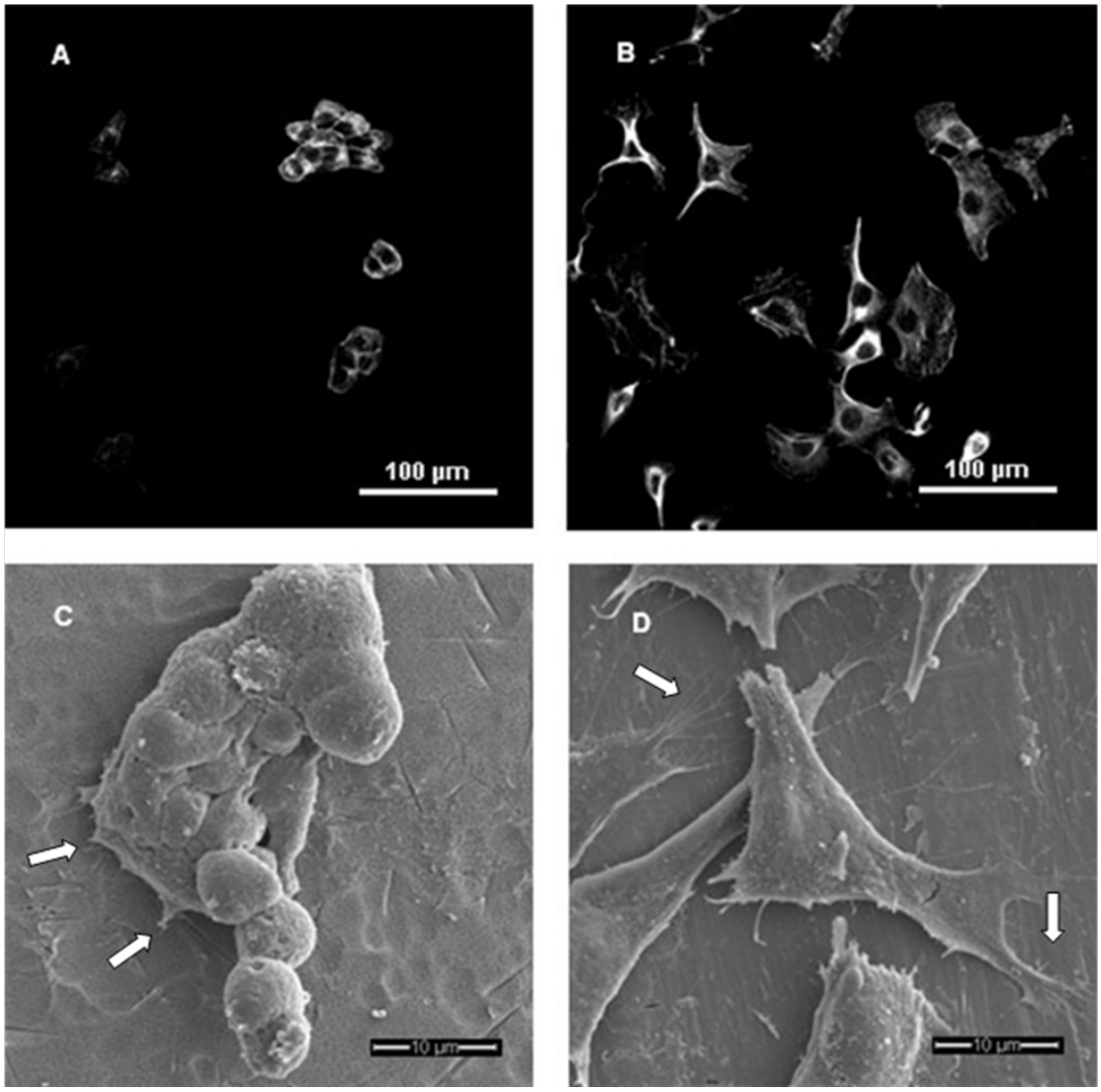

Figure 3.2: F-actin staining of MOVASs grown on (A) nanotubular TiO_2 versus (B) flat surfaces after 24 hours. SEM of cells on (C) nanotube surface and (D) flat surfaces. Arrows used to indicate extent and type of processes on nanotubular and flat surfaces.

To examine the link between nanotopography and proliferation further, cell cycle progression of ECs and VSMCs were examined using 5-ethynyl-2′-deoxyuridine (EdU), a thymidine analogue, which is incorporated by proliferating cells. EdU incorporation was measured after 24 and 72 hours in BAECs and MOVASs. The proportion of EdU positive BAECs increased initially on nanotubes, but returned to a level similar to that of the cells on flat surfaces by day 3. In contrast, the proportion of EdU positive MOVASs decreased significantly (Figure 3.3) over three days. This sustained decrease in proliferation is particularly relevant to stent applications since restenosis is directly caused by VSMC proliferation. In addition, restenosis is indirectly linked to the lack of re-endothelialization because an intact EC layer further promotes a non-proliferative and differentiated phenotype in VSMCs. These results suggest that the nanotubular surfaces may be capable of preferentially enhancing EC growth while decreasing VSMC proliferation.

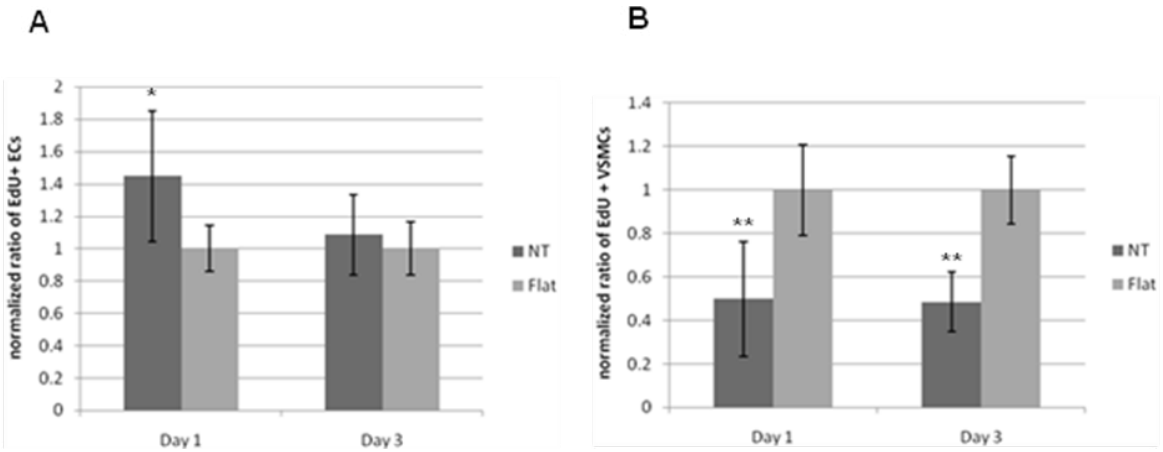

Figure 3.3: Ratio of EdU positive (A) ECs and (B) VSMCs on flat or nanotube (NT) substrate normalized by the average proportion of positive cells on flat surfaces on day 1 and 3. Data is presented as average ± standard deviation. *p<0.05, **p<0.01 vs. same day flat control, n=6.

Because VSMC proliferation is often associated with de-differentiation, maintaining a differentiated state may aid in preventing restenosis. Therefore, the effect that nanotopography has on the expression of smooth muscle α-actin (SMαA), a marker of differentiation,[27] was also investigated. MOVASs were grown on nanotubular and flat surfaces and harvested after 24 hours. To quantify the expression of SMαA, cell lysates from nanotube and flat surfaces were collected and analyzed through Western blotting. Cells grown on nanotubes versus flat surfaces showed increased SMαA expression (Figure 3.4) of approximately three fold as compared to controls. This suggests that nanotubes may help maintain the differentiated state of VSMCs, further reinforcing the non-proliferative phenotype.

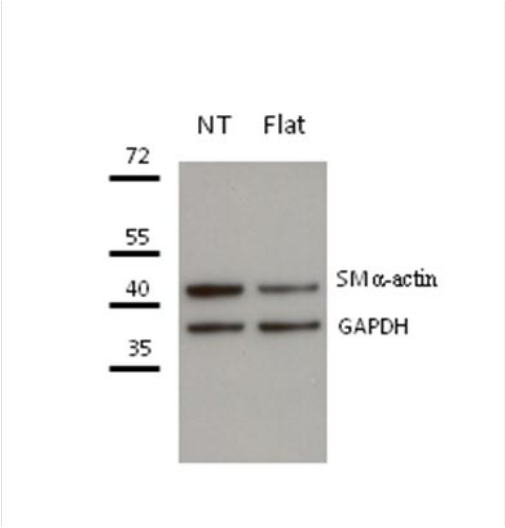

Figure 3.4: Western blot of smooth muscle α-actin (42 kDa) of MOVAS cells grown on nanotubular (NT) TiO_2 and flat surfaces after 24 hours. GAPDH (38 kDa) was used as a loading control.

In addition to effects on proliferation, the effects of nanotubes on the other functions of ECs were also explored. One primary function of ECs is the secretion of products that prevent clotting and inhibition of VSMC proliferation. Nitric oxide (NO) and Prostaglandin I_2 (PGI_2) are predominant products that act as anti-thrombogenic as well as anti-proliferative agents in VSMCs.[21, 28, 29] In a previous study, it was shown that

nanotubes did not significantly impact NO synthesis.[23] In this study, the ability of the nanotubes to affect PGI_2 secretion was investigated. Unlike the secretion of other anti-coagulants like heparan sulfate, which is controlled through the signaling of the glycocalyx on the apical side of ECs, PGI_2 secretion is regulated by integrin signaling on the basal side of the cell.[30] Hence, it was hypothesized that PGI_2 production may be increased through manipulation of the topography of the underlying surface. To test this hypothesis, BAECs were grown on the nanotube arrays and flat titanium for 24 hours. The supernatant of each condition was harvested and measured for PGI_2 concentrations using an EIA kit. Results show that nanotubes increased the production of PGI_2 by compared to flat titanium. When normalized by the average PGI_2 secreted by controls, ECs on nanotubes produced 1.4 ± 0.25 (average ± stdev) times the amount secreted by ECs on flat surfaces (1.0 ± 0.089). This difference was statistically significant ($n=9$, $p>0.005$). Furthermore, total protein secretion, as measured using a BCA assay, showed a slight increase in protein secretion on nanotubes samples, but this difference was not statistically significant. This suggests that the increase in PGI_2 was unlikely the result of global up-regulation of protein production. Rather, PGI_2 production can be selectively increased by the presence of extracellular matrix (ECM) proteins, such as laminin and fibronectin.[31] Since nanotube arrays have been shown to promote ECM production in ECs,[23] it is possible that increased PGI_2 is connected to increased ECM production. Regardless of the cause, enhancement of PGI_2 production is a very desirable stent quality. Because PGI_2 can reduce clotting while regulating VSMC differentiation, PGI_2 analogues have been suggested for use in the next generation of drug-eluting stents.[28] Therefore, a

surface that boosts endogenous production of this prostaglandin may represent a significant improvement to existing stent or vascular graft technologies.

CONCLUSION

Current clinically used modifications to bare metal stents are largely aimed at decreasing VSMC proliferation at the expense of EC proliferation, migration, and function. TiO_2 nanotubes represent a unique approach where a stent surface is modified to promote reendothelialization and decrease VSMC proliferation. The data from this study suggests that nanotopographical features can be used to promote proliferation and function in ECs and help VSMCs maintain their differentiated and non-proliferative phenotype. In particular, the enhanced production of PGI_2 is especially promising because the prostaglandin's ability to blunt thrombosis and restenosis. Reasons for a differential effect on proliferation in the two cell types is still unclear, and this may be due to the fact that nanotubes restrict the size of VSMCs but not ECs, as observed from immunostaining. Further study of how vascular cells respond to the different dimensions of nanotubes will help elucidate the mechanism behind such observed effects. This study has shown that TiO_2 nanotubes have a variety of desirable effects on both major cell types involved in repair after vascular injury and are a promising candidate for next generation vascular materials. This and future studies will aid in understanding how major processes involved in stent and vascular device implantation may be affected and modulated by topography, which would allow safer devices through better design.

CHAPTER 4: Microarray analysis of cells on nanotubes

INTRODUCTION

Current strategies to manage these restenosis and thrombosis risks in vascular devices such as drug-eluting stents are largely focused on blunting VSMC proliferation. However, these therapies are associated with a higher risk of late thrombosis[32] because drug-eluting coatings also inhibit EC function, migration, and proliferation, leading to poor re-endothelialization of the lumen.[33,34] Because ECs not only prevent coagulation but also VSMC proliferation,[21] rapid re-endothelialization and normal EC function is crucial to the success of any vascular implant. Thus, to minimize complications, an ideal stent should encourage EC migration, proliferation and function, while blunting VSMC proliferation.[35]

As suggested in previous chapters, titanium dioxide (TiO_2) nanotube arrays are a highly biocompatible material with precisely tunable dimensions. This control over nanotopographical dimensions allows for the fabrication of materials with feature sizes on the same order of magnitude as cell receptors or proteins and thus the ability to manipulate cell behavior through mechanical and topographical means.[36] Studies outlined in Chapter 3 suggest that the nanotubes may enhance EC motility,[23] proliferation, and function, while decreasing VSMC proliferation.[37] To further investigate the effects of nanotube arrays on vascular cells, microarray studies were performed to identify differentially expressed genes that may be responsible for the observed phenotypes.

METHODS

TiO_2 nanotube fabrication. TiO_2 nanotube arrays were formed via anodic oxidation in an electrolytic solution containing 0.2M Sodium Citrate Tribasic, 1M Sodium Hydrogen Sulfate, and 0.1M Potassium Fluoride, with Sodium Hydroxide added to adjust the pH of the solution. Titanium foil (0.25mm thick, 99.7% purity, Alfa Aesar) were anodized at a constant DC potential for 17 hours in a two-electrode electrochemical cell with a platinum foil as the counter electrode. The average length and pore diameter of the nanotubes were scaled by varying the pH of the electrolyte and the DC potential during anodization. Nanotubes 1 μm in length with an average pore diameter of 30 nm were prepared by anodization using 10 V bias in the 4 pH electrolyte. Nanotubes 1 μm in length with an average pore diameter of 100 nm were prepared by anodization using 20 V bias in a 2 pH electrolyte. All samples were subsequently rinsed in DI water and annealed at a temperature of 500 °C in oxygen ambient to crystallize the nanotubes. Heating and cooling rates of 1 °C/min were used with a dwell time of 6 hours. Surfaces were sterilized with 70% ethanol and UV prior to use in tissue culture.

HAEC and HAoSMC culture. Primary human aortic endothelial cells (HAECs) and primary human vascular smooth muscle cells (HAoSMCs) (Lonza, Walkersville, MD) were cultured according to manufacturer's instructions using Lonza's HAEC and HAoSMC complete media. The cells were cultured in a humidified 95% air/5% CO_2 incubator at 37°C. Cells used in this experiment were passaged less than 15 times.

RNA isolation for microarray. HAECs and HAoSMCs were seeded at 5×10^4 cells/cm^2 on flat and nanotube substrates. Cells were harvested after 24 hours using

Qiagen's RNeasy kit (Valencia, CA) according to manufacturer's instructions. Concentration and purity of isolated RNA was measured using a NanoDrop spectrophotometer (Thermo Fisher Scientific, Wilmington, DE)

Microarray. Sample preparation, labeling, and array hybridizations were performed according to standard protocols from the UCSF Shared Microarray Core Facilities and Agilent Technologies (http://www.arrays.ucsf.edu and http://www.agilent.com). Total RNA quality was assessed using a Pico Chip on an Agilent 2100 Bioanalyzer (Agilent Technologies, Palo Alto, CA). RNA was amplified and labeled with Cy3-CTP using the Agilent low RNA input fluorescent linear amplification kits following the manufacturers protocol. Labeled cRNA was assessed using the Nanodrop ND-100 (Thermo Fisher Scientific), and equal amounts of Cy3 labeled target were hybridized to Agilent whole human genome 4x44K Ink-jet arrays. Hybridizations were performed for 14 hrs, according to the manufacturer's protocol. Arrays were scanned using the Agilent microarray scanner and raw signal intensities were extracted with Feature Extraction v10.1 software. A total of 19 arrays were hybridized and represent 4 biological replicates for each group (with the exception of group VSMC-NT30, which has 3 biological replicates).

Differential expression analysis. The following terminology is used to discuss the results of our analysis:

M – $\log_2$ (S2/S1). Log 2 based fold change of entity of interest. M=1 means two-fold increase in S2 compared to S1. M=0 means equal expression. M=-1 means 2 fold down-regulation.

aveA–average $\log_2$ based intensity of the same probe across all arrays, a proxy for gene expression level

B - log posterior odds ratios, ratio between the probability that a given gene is **differentially expressed (DE)** over the probability that a given gene is not differentially expressed; B≥0 means equal or more probability that a gene is DE than non-DE.[38]

FDR – False Discovery Rate, which is the percentage of falsely declared DE genes among the set of declared DE genes. A FDR cutoff of 0.01 indicates that 1% of the declared DE genes are expected to false positives.[39]

AdjP – Adjusted p-value, which controls for family-wise error rates, the probability of having more than one false discovery. An adjusted p-value cutoff of 0.01 indicates that the declared DE set has 1% chance to have more than one false positive.

Raw log-intensities are normalized using *quantile* normalization method that is proposed by Bolstad *et al*.[40] No background subtraction was performed, and the median feature pixel intensity was used as the raw signal before normalization.

A one-way ANOVA model is formulated and specific contrasts are formulated to examine the two pairwise comparisons of interest. Moderated t-statistic, B statistic, false discovery rate and p-value for each gene were obtained. Adjusted p-values were produced by the method proposed by Holm.[41] All procedures were carried out using functions in the R package *limma in Bioconductor*.[42, 43] Shortlists for HAECs were generated using the criteria of $B \geq 0$ and Nominal $P \leq 0.001$. Shortlists for HAoSMCs

were generated using the criteria of $B > 0$, Nominal $P \leq 0.001$, and fold-change > 2 (i.e. absolute value of $\log_2$ fold-change > 1).

Microarray data has been submitted to the GEO (accession number: GSE17676) and can be found at the following address:

http://www.ncbi.nlm.nih.gov/geo/query/acc.cgi?token=zhinfukqcyiqebk&acc=GSE17676

Quantitative Polymerase Chain Reaction. For confirmation of microarray data, cells were seeded at 5 x 10^4 cells/cm^2 on flat and nanotube surfaces. In addition, ECs were also seeded at 5 x 10^3 cells/cm^2 for low density experiments. After 24 hours, samples were harvested using Ambion/Applied Biosystems's Cell to C_T kit (Foster City, CA). Lysis, RT-PCR, and qPCR were performed according to manufacturer's instructions using a StepOne Plus instrument (Applied Biosystems). Primers for each target were designed by Primer Express 3.0 software (Applied Biosystems) or obtained from the National Cancer Institute's Quantitative PCR Primer Database (http://web.ncifcrf.gov/rtp/gel/primerdb/) for the following genes: FST (forward primer – 5'-CAGTAAGTCGGATGAGCCTGTCT, reverse primer – 5'-CAGCTTCCTTCATGGCACACT), ATF3 (forward – 5'-CTGCCCGCCTTTCATCTG, reverse – 5'-CAGACACTGCTGCCTGAATCC), EGR1 (forward – 5'-TTTGCCAGGAGCGATGAAC, reverse – 5'-CCGAAGAGGCCACAACACTT), YAP1 (forward – 5'-CGTCCAGCAAGATACTTTAATCCTCTAT, reverse – 5'-CTGTGAAAGAGGTCAGCAATACATT), and GAPDH (forward – 5'-TGCACCACCAACTGCTTAGC, reverse – 5'-GGCATGGACTGTGGTCATGAG).

Each experimental condition was performed three times (n=3). Expression levels of the genes were measured in technical triplicates.

RESULTS AND DISCUSSION

Given the dual role ECs play in preventing both coagulation and VSMC proliferation, the effect of nanotopography on EC gene expression was first examined. Previous studies have suggested that cells may be sensitive to nanotube dimensions, and that certain tube diameters may enhance survival, proliferation, differentiation, or migration.[23, 44-46] To explore the effect of nanotube diameter on ECs, primary human aortic endothelial cells (HAECs) were grown on smooth surfaces as well as 30 nm and 100 nm nanotube arrays. mRNA transcripts from the cells were harvested after 24 hours and expression levels were probed using whole-genome microarrays. Analysis of the arrays revealed no significant differences between ECs exposed to the 30 nm and 100 nm nanotube arrays, but significant differences in over 100 transcripts between nanotube arrays and flat surfaces. The lack of significant differences between cells exposed to the 30 and 100 nm arrays in this experiment may be due to the differences in cell types or origin that were used in this study versus previous studies (e.g. bovine aortic ECs[23] and mesenchymal cells[47] vs. primary HAECs) as well as variation in the duration of exposure to the nanotube array surfaces before a cellular response was measured. It is also feasible that cells may be responding to different nanotopographical dimensions via protein or enzymatic control rather than transcriptional regulation. However, our data does suggest that primary HAECs are not responsive (at least not transcriptionally) to variation in nanotube diameters in the 30-100 nm range after 24 hours of exposure.

Genes with significant differences in expression between the nanotubular and flat substrates were analyzed using Ingenuity Pathway Analysis (IPA) software to identify altered cellular processes and functions due to exposure to nanotubes. From the data, IPA identified over 50 genes with sufficient published information to sort into various functional categories. These categories were further classified according to their likely impact on processes relevant to performance of a vascular implant (Figure 4.1A). Sorting resulted in four major groups of genes whose changes in expression levels would likely indicate an alteration in proliferation, migration, cell death, and inflammation or coagulation (i.e EC activation, which results in recruitment of leukocytes or platelets, or progression of the inflammatory response or coagulation cascade). The genes were then further classified by whether their expression would likely promote or inhibit the relevant processes (i.e. proliferation, migration, cell death, and inflammation) using IPA's curated findings and plotted in Figure 4.1B (see supplemental section, Table S1 for additional information). Log_2-fold changes in expression of genes that promote a process were plotted according to the y-axis on the left such that an upregulation of a gene in this category would appear on the top half of the graph. Genes that inhibit that same process were plotted according to y-axis on the right such that downregulation of a gene that retards a process would also appear on the top half of the plot. Organized this way, genes that appear on the top half of the plot would likely promote one of the processes while genes that appear on the bottom half of the plot would contribute to the inhibition of the process. The expression patterns of the genes suggest that ECs exposed to nanotubes are more proliferative, with 15 genes whose expression patterns that were more consistent with a proliferative phenotype and 5 more consistent with a non-proliferative phenotype.

The cells also appear to be more motile (7 genes that promote the process versus 2 that inhibit). Further, ECs on nanotube arrays also seemed more resistant to cell death (3 promote versus 9 inhibit) and activation (1 promote versus 6 inhibit).

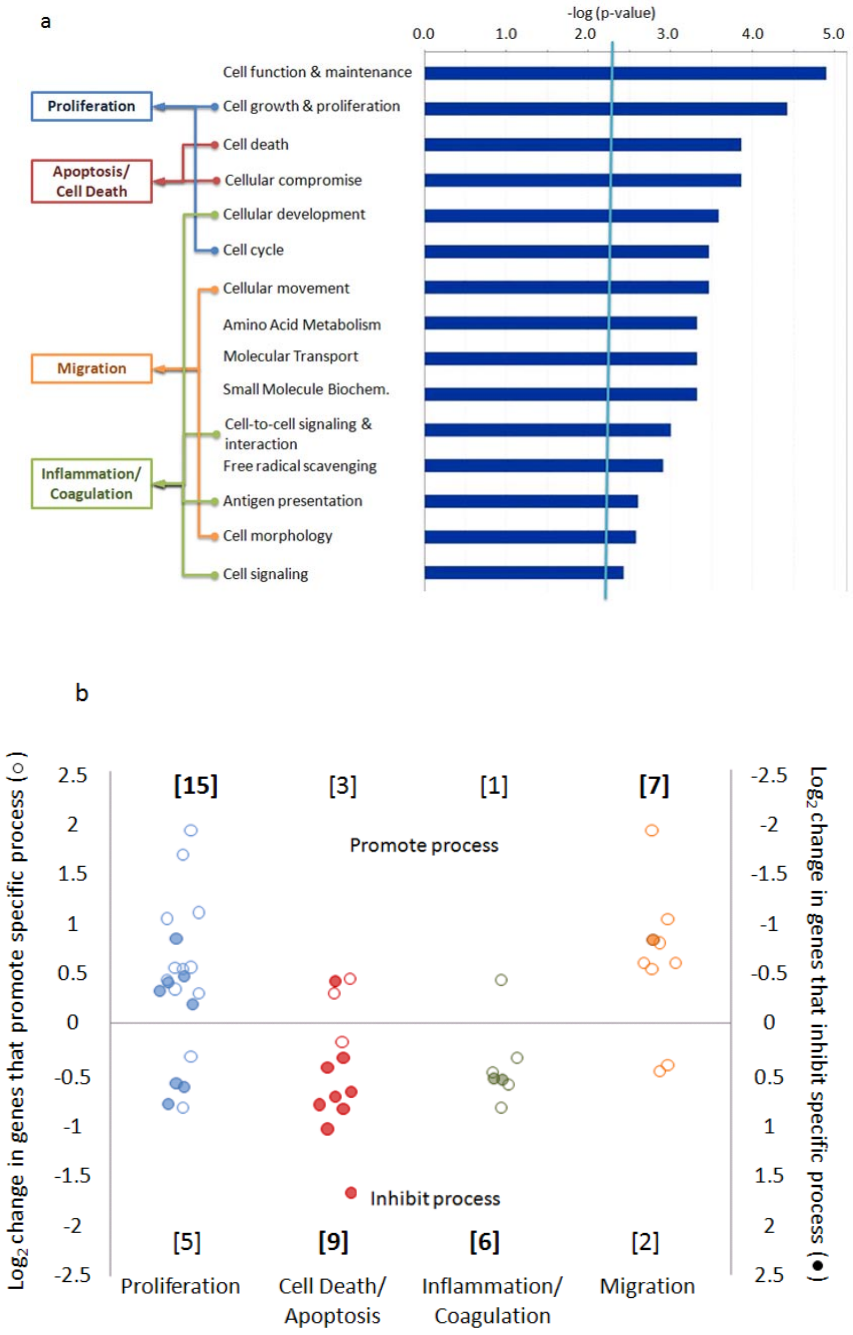

Figure 4.1: Nanotube effects on cellular functions and processes of ECs. List of significantly affected cellular functions identified by Ingenuity Pathway Analysis with $p<0.005$ **(A).** Identified functions are sorted into processes relevant to vascular device performance. Genes whose expression is significantly affected by nanotube arrays are plotted according to their likely effects on the four processes **(B)**. Genes that promote a process are represented by open circles (o) with their y-axis on the left, while genes that inhibit a process are represented by filled-in circles (•) and have their y-axis on the right. Plotted this way, genes whose expression pattern is likely to promote a specific process (e.g. enhanced expression of a promoter of proliferation or reduced expression of a gene that inhibits proliferation) will appear on the top half of the graph, and those who would likely inhibit the process would appear on the bottom. Numbers at the top and bottom denote the number of genes that appear on the top or bottom region of the graph. For example, there are 15 EC genes whose expression pattern is consistent with a proliferative phenotype.

This data is consistent with previous reports about the ability of nanotubes to promote endothelial cell proliferation and migration. Our group has observed increased DNA synthesis in ECs exposed to nanotube arrays as compared to flat surfaces.[37] The pro-migratory effects of the nanotubes have also been shown through analysis of cell morphology, focal adhesion staining, and scratch migration assays.[23, 37] Microarray analysis from this study not only supports previous functional data but also provides possible gene candidates that are involved in these responses.

While the pro- proliferative and migratory effects of the nanotubes revealed through microarray analysis are consistent with prior reports, the anti- cell death and activation aspects of the nanotopography are novel findings. In fact, previous studies suggest that increased surface roughness in stainless steel surfaces may increase activation of ECs, increasing expression of cell adhesion molecules such as E-selectin and VCAM-1.[48] However, despite the increased roughness of nanotube arrays in comparison to flat surfaces, our microarray analysis revealed no significant changes those particular molecules and decreases in other markers of activation. The discrepancy in EC activation in these studies may stem from the difference in chemical composition, order of the substrates, or a combination of both. TiO_2 is a highly inert material but stainless steel is an alloy with some elements, such as nickel,[49] that are more immunogenic. Increased roughness likely increases the surface area of the substrate in contact with cells. Cells on a slightly more immunogenic surface, like stainless steel, would see a higher amount of inflammatory stimuli on a roughened surface, whereas cells on an inert surface such as TiO_2 would not. Furthermore, stainless steel substrates used in previous experiments had a random topography, whereas nanotube arrays used in these experiments were highly

ordered. In addition to the changes in these processes, the microarrays also identified molecular networks that are most likely altered by the nanotubes as well as probable genes that are correlated with the differences in phenotype. The top network identified by IPA (Figure 4.2) contained members such as nuclear factor-kappa ß (NF-κB), activator protein-1 (AP-1), mitogen-activated protein kinases (MAPKs), which have previously been implicated in mechanotransduction[50] and sensing of shear stress in endothelial cells.[51] The appearance of these genes in this network suggest that ECs may be sensing nanotopographic cues through proteins upstream of these signaling molecules, such as integrins, mechanosensitive ion channels, cell surface proteoglycans, or other shear-sensitive elements. NF-κB, for example, has been shown to be activated via Rac1 in response to integrin activation.[52] AP-1 is another transcription factor that been implicated in integrin-mediated responses to mechanical cues via ERK1/2 phosphorylation.[53] Detailed examination of genes most profoundly affected by nanotopography reviewed that transcripts for follistatin (FST), a gene expressed in migrating and proliferating ECs,[54] experienced the greatest absolute $\log_2$ fold change in expression. ECs exposed to nanotubes produced nearly 4 times more FST ($\log_2$ fold change = +1.91) than cells on flat controls. This change in follistatin expression was also confirmed by quantitative PCR (qPCR), which yielded expression levels consistent with that of the microarrays, with a $\log_2$ fold change of $+2.48 \pm 0.46$ relative to flat controls. In ECs, follistatin, an activin-binding autocrine/paracrine protein, regulates proliferation by inhibiting the anti-proliferatory effects of activin.[55, 56] While there have been studies about the how EC FST expression is regulated via chemical cues, such as with heparin,[57-59] little is known about how the gene can be regulated by mechanical cues. However, in

our study, follistatin serves as a marker for EC proliferation and migration, and its expression pattern, as well as those of other genes (see Table S1), supports the upregulation of these two processes in ECs exposed to nanotopographical cues.

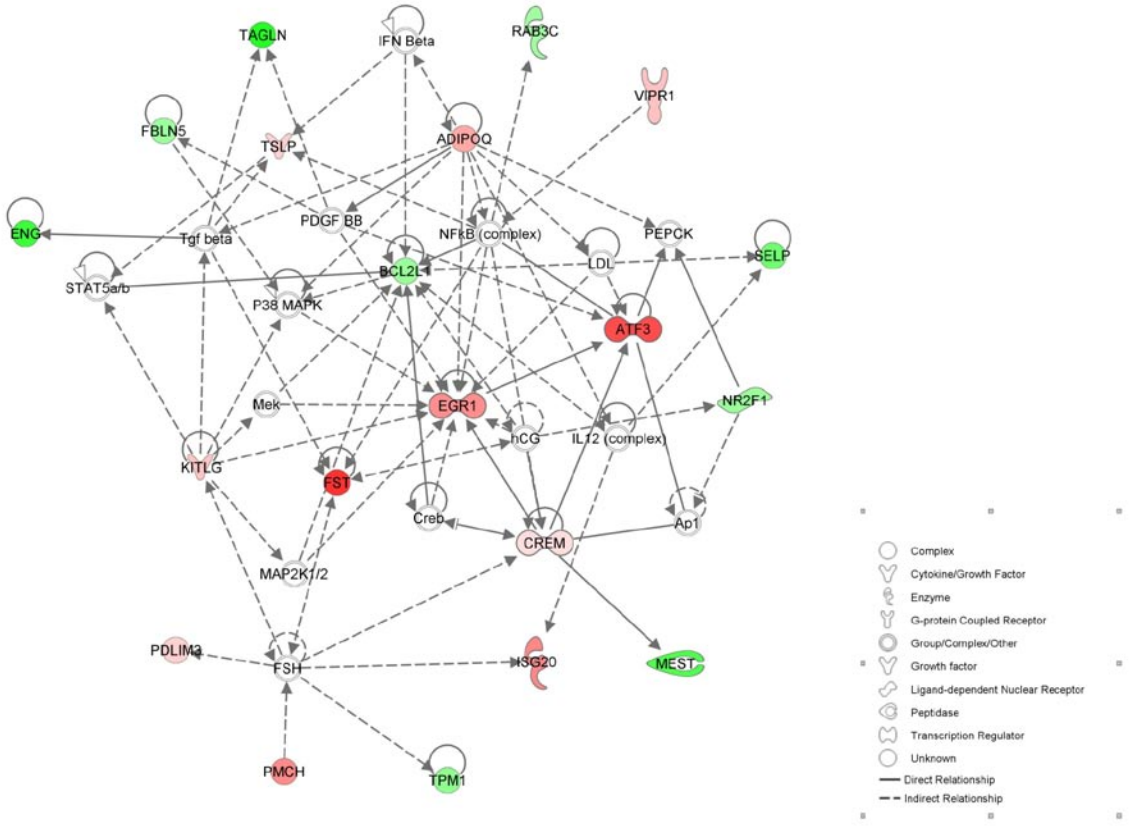

Figure 4.2: Top network of genes in ECs whose expression are significantly affected by exposure to nanotube arrays. Red indicates upregulation, green indicates downregulation. Intensity of color is proportional to magnitude of change. For the sake of simplicity, relationships between genes without a significant change in expression are not shown. See original network map in supplemental section, Figure S2.

Initially after a vascular device like a stent is implanted, the EC layer is denuded and the implant surface is either bare or sparsely covered with ECs. To see if similar expression patterns might also be observed in this initial stage, ECs were seeded on nanotube and flat substrates at low densities. After 24 hours, expression of several genes identified by microarray analysis was measured by qPCR. In addition to FST, activating transcription factor 3 (ATF3) was chosen because it had the next largest absolute $\log_2$

fold change, is expressed in proliferating cells,[60] and plays a role in promoting cell survival.[61] Early growth response 1 (EGR1) expression was also examined because of its established role as a transcription factor in mechanotransduction and extracellular matrix sensing.[62] Quantitative PCR results indicated that ECs grown at low densities also showed increased expression of FST, ATF3, and EGR1. While increase in expression of FST remained at about 4 fold (+2.03 ± 0.18 $\log_2$ fold change), the expression levels of ATF3 and EGR1 increased dramatically (+3.63 ± 0.35 and +3.62 ± 0.44 $\log_2$ fold change, respectively) at even higher levels than shown on the microarrays (Figure 4.3). This data suggests that during the initial stages post implantation, nanotube surface would have an even more profound effect than predicted by microarray.

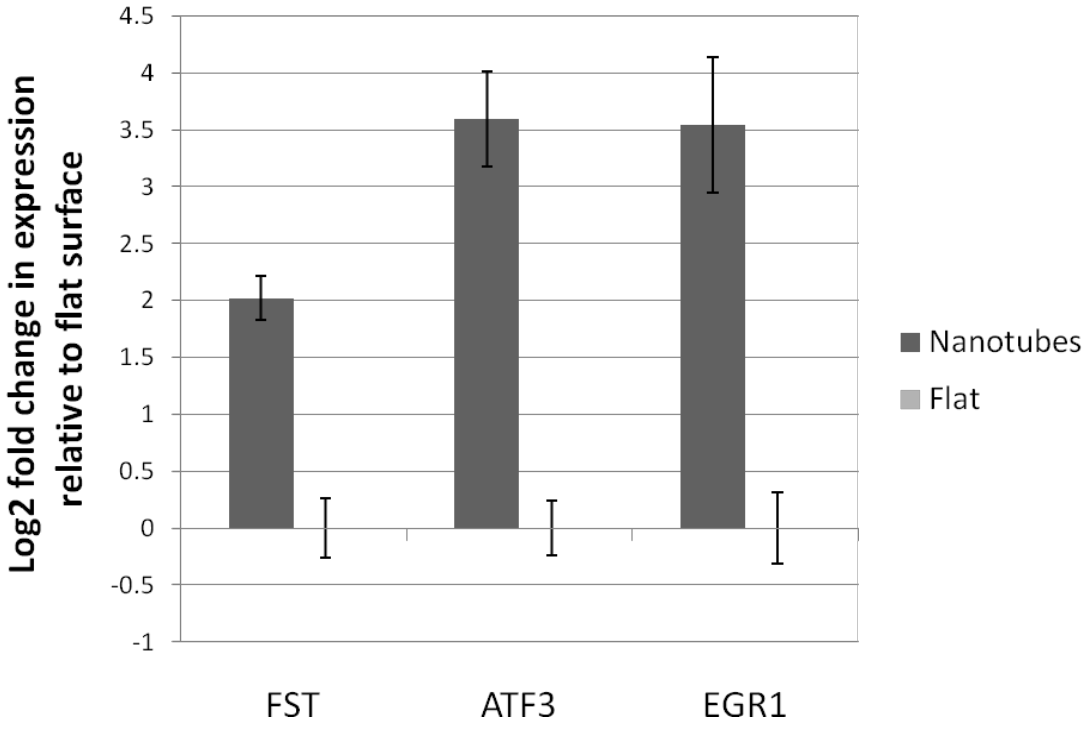

Figure 4.3: Average expression levels of follistatin (FST), activating transcription factor 3 (ATF3), and early growth response 1 (EGR1) in ECs grown at low densities measured by quantitative PCR. Data is normalized by expression levels of each gene by ECs on flat surfaces and presented as average ± standard deviation. * $p<0.05$ when compared to flat controls, n=3.

In addition to ECs, most vascular implants will interact with VSMCs. Uncontrolled proliferation of these cells after implantation often results in complications such as restenosis or device failure. Therefore, it is crucial to have a detailed understanding of how VSMCs interact with any possible vascular device coating. Thus, in addition to studying EC behavior, we also examined VSMC response to nanotube arrays. Because nanotubes of 30 nm and 100 nm in diameter did not seem to elicit a significant difference in EC behavior, only the 30 nm arrays were used to investigate VSMC behavior. VSMCs were seeded onto 30 nm nanotube arrays and flat surfaces for 24 hours. Like ECs, VSMCs were then harvested after 24 hours and gene expression of the entire genome was probed using microarrays. Top hits were filtered by p-value and absolute $\log_2$ fold change values to generate a shortlist of over 170 genes. The most significantly changed cellular functions were identified using IPA. Significantly affected functions were further grouped into categories relevant to the performance of vascular devices, which yielded the same four processes as ECs: proliferation, cell death, inflammation, and migration (Figure 4.4A). Genes were then sorted according to whether they were likely to up- or down-regulate these four processes and plotted in the same manner as ECs such that genes whose expression patterns would like promote a process would appear as data points on the top half of the graph, while those that would likely inhibit the process would appear on the bottom half (Figure 4.4B). In contrast to ECs, genes significantly changed in VSMCs were not the same genes differentially expressed in ECs. In fact, plot of the $\log_2$ fold change of all genes for ECs versus VSMCs suggest that TiO_2 nanotubes have divergent effects on the two cell population (Figure S1). Moreover, expression patterns in VSMCs in contact with the nanotube arrays strongly suggest a less

proliferative (7 promote versus 33 inhibit) phenotype. While the number of genes whose expression would likely inhibit versus promote cell death (14 promote versus 17 inhibit) and migration (6 promote versus 9 inhibit) are less striking, the expression pattern of genes involved in inflammation or coagulation seem to indicate a less activated phenotype (3 promote versus 9 inhibit).

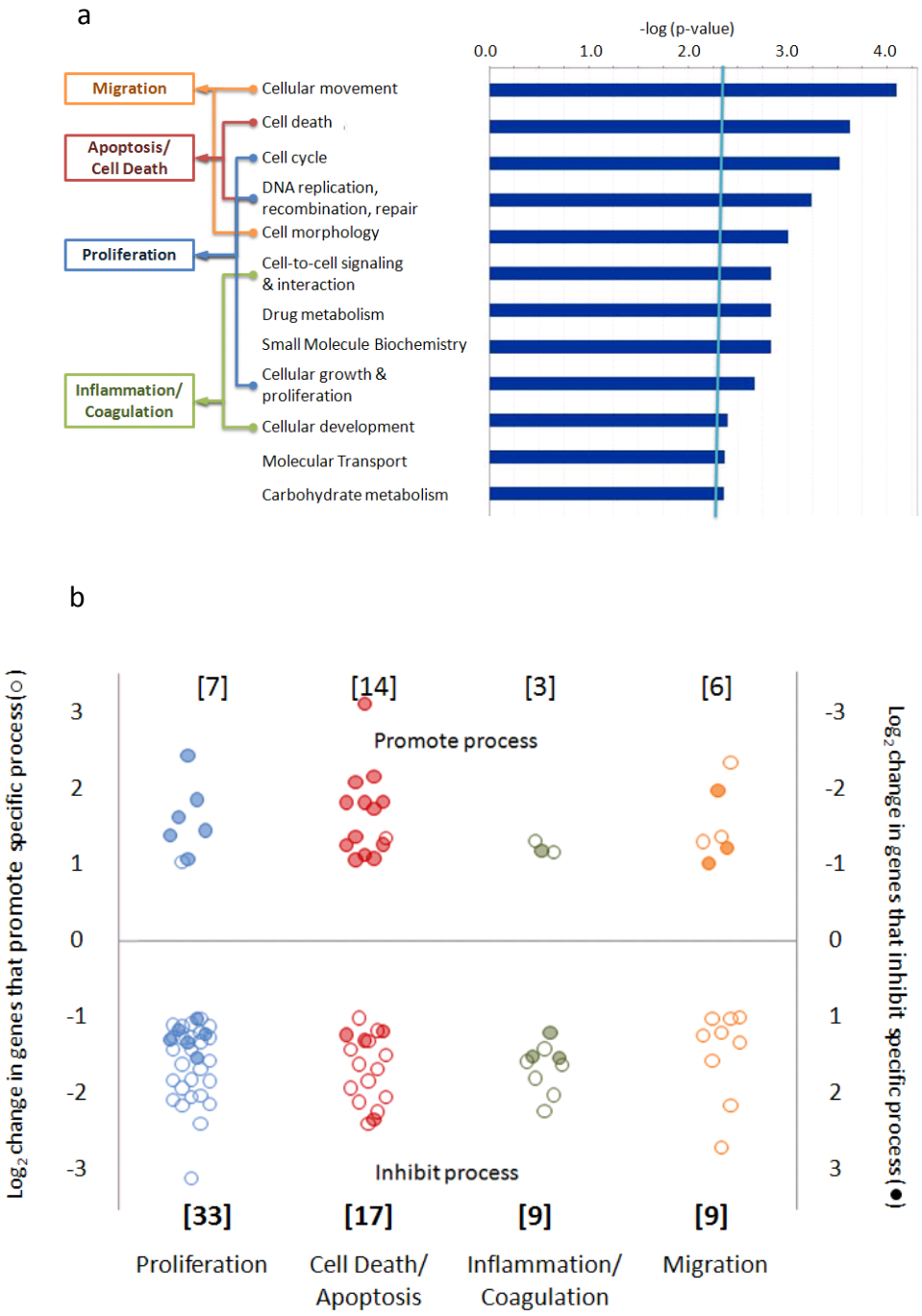

Figure 4.4: Nanotube effects on cellular functions and processes of VSMCs. **(A)** List of significantly affected cellular functions identified by Ingenuity Pathway Analysis with $p<0.005$. Identified functions are sorted into processes relevant to vascular device performance. Genes whose expression is significantly affected by nanotube arrays are plotted according to their likely effects on the four processes **(B)**, see figure 1 for more detailed explanation. Numbers at the top and bottom denote the number of genes that appear on the top or bottom region of the graph. For example, there are 33 genes whose expression patterns is consistent with a less proliferative phenotype.

Analysis of microarray data also yielded top networks and a set of genes most significantly affected by the nanotopography. Some members of the top network, such as NF-κB and AP-1 overlapped with the results from the top EC network (Figure 4.5) suggesting that similar signaling pathways may be involved in EC and VSMC sensing of the nano-environment. However, differential modulation of these pathways may lead to differential regulation of key transcription factors, resulting in divergent responses to the same substrate. The greatest absolute $\log_2$ fold change in expression was in YAP1, or Yes-associated protein 1, a gene that has been associated with increased proliferation and decreased apoptosis.[63] YAP1 expression was confirmed by qPCR, which showed a decrease in gene expression, but to a lesser degree than the level demonstrated by microarray ($\log_2$ fold change= -0.96 ± 0.33). Surprisingly, the expression of smooth muscle α-actin (SMαA), a marker of differentiation previously shown to be downregulated in mouse VSMCs exposed to nanotubes,[37] did not see a significant change in expression in this study. This may be due to the different cell origin and type used in the two studies. Previous data was collected with an immortalized mouse cell line, which can behave quite differently from primary human cells. Notably, the growth rate of the mouse cell line was much higher so it is possible that differences in SMαA expression had not yet occurred when the human cells were harvested for microarray. Nevertheless, data from this study strongly supports the idea that nanotube arrays have an anti-proliferatory effect on VSMCs, an effect crucial to inhibiting restenosis in an ideal stent or vascular device.

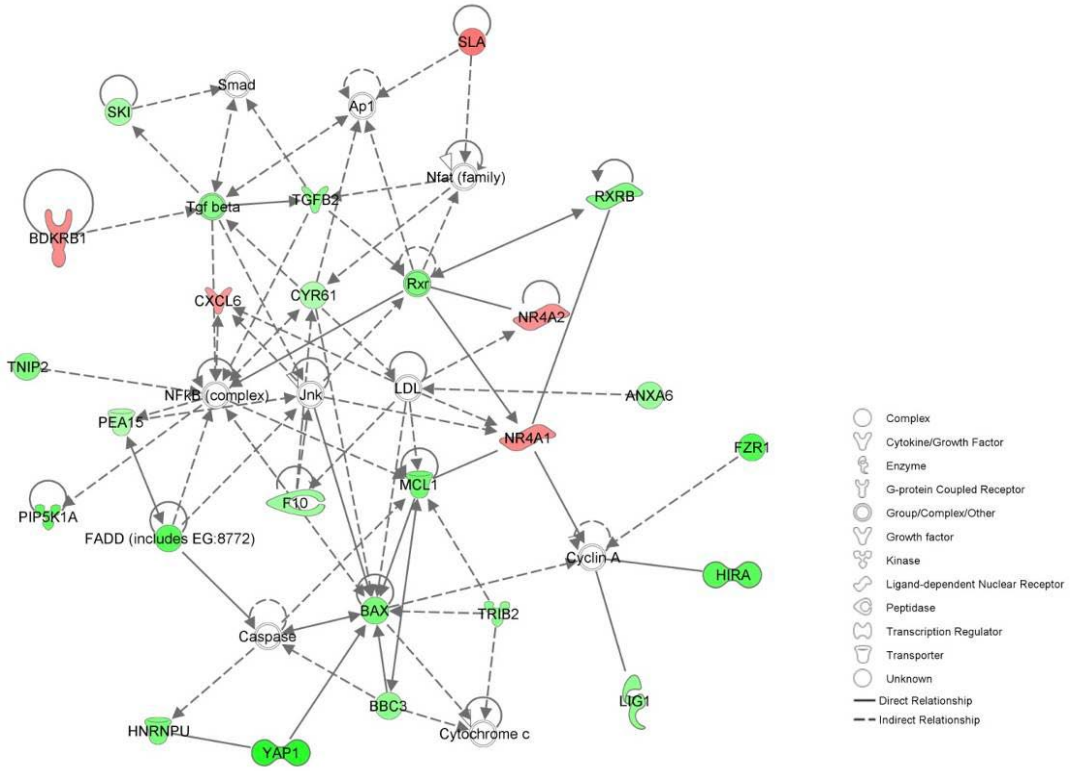

Figure 4.5: Top network of genes in VSMCs whose expression are significantly affected by exposure to nanotube arrays. Red indicates upregulation, green indicates downregulation. Intensity of color is proportional to magnitude of change. For the sake of simplicity, relationships between genes without a significant change in expression are not shown. See original network map in supplemental section, Figure S3.

Existing strategies of reducing vascular device complications are largely aimed at preventing restenosis at the expense of reendothelialization. The ideal vascular implant, however, should prevent VSMC proliferation and encourage EC proliferation, migration, and quiescence. Data from this and previous studies suggest that TiO_2 nanotube arrays may be a promising candidate for a next-generation stent or vascular device coating as because of the divergent response of ECs and VSMCs to the material. In addition, this study also identified genes and possible pathways that are correlated with changes in EC and VSMC phenotype. Identifying the genes and networks associated with phenotype

changes in response to nanotopographical cues maybe a crucial step toward understanding how cells sense and respond to nanotopography and how these interactions can be used to improve medical device design.

CHAPTER 5: Conclusions and Future Directions

The results from this project suggest that nanotopographical surfaces can interact with small molecules, proteins, and cells in a way that may have applications for local drug delivery or vascular device improvement. Findings in the first part of this work show that nanotubular TiO_2 is amenable to small molecule drug elution for a week and protein delivery for a month. This duration of release makes the material a feasible candidate for a drug eluting coating in clinical applications such as dental, bone, or vascular implants. Results from the second part of this dissertation show that varying cell types can respond differently to the same nanotopographical cue. In vascular cells, nanotubes increased proliferation and function in endothelial cells but decreased proliferation in vascular smooth muscle cells. We traced phenotypic responses to changes in gene expression in cells and identified possible candidates that may be involved in mediating this response. These findings suggest that nanotopography can change gene expression via different mechanisms in different cell types in a manner that may have clinical utility.

Traditionally, the field of cell biology has largely focused upon how cells respond to chemical cues. Recently, this focus has expanded to include how cells respond to mechanical forces and spatial cues. This work represents one of the first attempts to understand how nanotopographical cues impact cell behavior from gene expression to phenotypic changes. This work is by no means complete. Future studies in this area can be divided into two directions: (1) optimization and testing of the material for drug elution and/or vascular device applications in animal models and (2) elucidating our

understanding the mechanism of interaction between nanomaterials and small molecules, proteins, or cells.

Because the results from drug elution studies suggest that this technology is sufficiently close to being clinically useful, further optimization would be warranted so that that material could extend drug delivery duration or capacity. This would include exploring different shapes or dimensions of the nanotubes and varying surface treatments or drug loading methods. Varying these parameters would not only optimize drug elution but also provide insight into the mechanism of drug retention and release on the nanoscale.

Aside from drug loaded nanotubes, future directions could include investigating of the "pro-healing" effects of unloaded nanotubes can translate into significant effects *in vivo*. In addition, the data generated from microarray experiments have identified potential candidates that could be responsible for the phenotypic changes we see in vascular cells. Future investigation in this area would elucidate these nano-sensing pathways, which could provide valuable information about the mechanisms behind cellular interaction with nanomaterials.

CHAPTER 6: References

1. Bennett, M. R. *Heart* **2007,** 93, (8), 895-6.
2. Wieneke, H.; Dirsch, O.; Sawitowski, T.; Gu, Y. L.; Brauer, H.; Dahmen, U.; Fischer, A.; Wnendt, S.; Erbel, R. *Catheterization and Cardiovascular Interventions* **2003,** 60, (3), 399-407.
3. Wessely, R. *Arteriosclerosis Thrombosis and Vascular Biology* **2005,** 25, (8), E130-E130.
4. Kollum, M.; Farb, A.; Schreiber, R.; Terfera, K.; Arab, A.; Geist, A.; Haberstroh, J.; Wnendt, S.; Virmani, R.; Hehrlein, C. *Catheterization and Cardiovascular Interventions* **2005,** 64, (1), 85-90.
5. Sigler, M.; Paul, T.; Grabitz, R. G. *Zeitschrift Fur Kardiologie* **2005,** 94, (6), 383-+.
6. Liu, J. X.; Yang, D. Z.; Shi, F.; Cai, Y. J. *Thin Solid Films* **2003,** 429, (1-2), 225-230.
7. Yoriya, S.; Mor, G. K.; Sharma, S.; Grimes, C. A. *Journal of Materials Chemistry* **2008,** 18, (28), 3332-3336.
8. Paulose, M.; Prakasam, H.; Varghese, O.; Peng, L.; Popat, K.; Mor, G.; Desai, T.; Grimes, C. *J PHYS CHEM C* **2007,** 111, (41), 14992-14997.
9. Prakasam, H. E.; Shankar, K.; Paulose, M.; Varghese, O. K.; Grimes, C. A. *J PHYS CHEM C* **2007,** 111, (20), 7235-7241.
10. Cai, Q. Y.; Paulose, M.; Varghese, O. K.; Grimes, C. A. *Journal of Materials Research* **2005,** 20, (1), 230-236.
11. Ainslie, K. M. T., S.L.; Popat, K.C.; Desai T.A. *J Biomed Mater Res A* **2008**.
12. Park, J.; Bauer, S.; von der Mark, K.; Schmuki, P. *Nano Lett* **2007,** 7, (6), 1686-91.
13. Popat, K.; Leoni, L.; Grimes, C.; Desai, T. *BIOMATERIALS* **2007,** 28, (21), 3188-3197.
14. Popat, K.; Eltgroth, M.; La Tempa, T.; Grimes, C.; Desai, T. *SMALL* **2007,** 3, (11), 1878-1881.
15. Popat, K.; Eltgroth, M.; LaTempa, T.; Grimes, C.; Desai, T. *BIOMATERIALS* **2007,** 28, (32), 4880-4888.
16. Kim, D.; Macak, J. M.; Schimidt-Stein, F.; Schmuki, P. *Nanotechnology* **2008,** 19, (30), -.
17. American Heart Association, Heart Disease and Stroke Statistics: 2007 Update At-a-Glance. In 2007; p 36.
18. Kubicek, J. D.; Brelsford, S.; Ahluwalia, P.; Leduc, P. R. *Langmuir* **2004,** 20, (26), 11552-6.
19. Dalby, M. J.; Pasqui, D.; Affrossman, S. *IEE Proc Nanobiotechnol* **2004,** 151, (2), 53-61.
20. Choudhary, S.; Haberstroh, K. M.; Webster, T. J. *Tissue Eng* **2007,** 13, (7), 1421-30.
21. Rzucidlo, E. M.; Martin, K. A.; Powell, R. J. *J Vasc Surg* **2007,** 45 Suppl A, A25-32.

22. Yim, E. K.; Reano, R. M.; Pang, S. W.; Yee, A. F.; Chen, C. S.; Leong, K. W. *BIOMATERIALS* **2005,** 26, (26), 5405-13.
23. Brammer, K. S.; Oh, S.; Gallagher, J. O.; Jin, S. *Nano Lett* **2008,** 8, (3), 786-93.
24. Sato, M.; Ohashi, T. *Biorheology* **2005,** 42, (6), 421-41.
25. Tanaka, M.; Takayama, A.; Ito, E.; Sunami, H.; Yamamoto, S.; Shimomura, M. *J Nanosci Nanotechnol* **2007,** 7, (3), 763-72.
26. McGrath, J. L.; Osborn, E. A.; Tardy, Y. S.; Dewey, C. F., Jr.; Hartwig, J. H. *Proc Natl Acad Sci U S A* **2000,** 97, (12), 6532-7.
27. Owens, G. K.; Kumar, M. S.; Wamhoff, B. R. *Physiol Rev* **2004,** 84, (3), 767-801.
28. McCormick, C.; Wadsworth, R. M.; Jones, R. L.; Kennedy, S. *Biochem Soc Trans* **2007,** 35, (Pt 5), 910-1.
29. Newby, A. C.; Southgate, K. M.; Assender, J. W. *Herz* **1992,** 17, (5), 291-9.
30. Pahakis, M. Y.; Kosky, J. R.; Dull, R. O.; Tarbell, J. M. *Biochem Biophys Res Commun* **2007,** 355, (1), 228-33.
31. Balcells, M.; Edelman, E. R. *J Cell Physiol* **2002,** 191, (2), 155-61.
32. Shuchman, M. *N Engl J Med* **2006,** 355, (19), 1949-52.
33. Steffel, J.; Tanner, F. C. *Herz* **2007,** 32, (4), 268-273.
34. Finn, A. V.; Joner, M.; Nakazawa, G.; Kolodgie, F.; Newell, J.; John, M. C.; Gold, H. K.; Virmani, R. *Circulation* **2007,** 115, (18), 2435-41.
35. Ako, J.; Bonneau, H. N.; Honda, Y.; Fitzgerald, P. J. *American Journal of Cardiology* **2007,** 100, (8B), 3M-9M.
36. Leduc, P. R.; Robinson, D. N. *Advanced Materials* **2007,** 19, (22), 3761-3770.
37. Peng, L.; Eltgroth, M. L.; LaTempa, T. J.; Grimes, C. A.; Desai, T. A. *BIOMATERIALS* **2009,** 30, (7), 1268-1272.
38. Lonnstedt, I.; Speed, T. *Statistica Sinica* **2002,** 12, (1), 31-46.
39. Benjamini, Y.; Hochberg, Y. *Journal of the Royal Statistical Society Series B-Methodological* **1995,** 57, (1), 289-300.
40. Bolstad, B. M.; Irizarry, R. A.; Astrand, M.; Speed, T. P. *Bioinformatics* **2003,** 19, (2), 185-93.
41. Holm, S. *Scandinavian Journal of Statistics* **1979**, (6), 65-70.
42. Smyth, G. K. *Stat Appl Genet Mol Biol* **2004,** 3, Article3.
43. Gentleman, R. C.; Carey, V. J.; Bates, D. M.; Bolstad, B.; Dettling, M.; Dudoit, S.; Ellis, B.; Gautier, L.; Ge, Y.; Gentry, J.; Hornik, K.; Hothorn, T.; Huber, W.; Iacus, S.; Irizarry, R.; Leisch, F.; Li, C.; Maechler, M.; Rossini, A. J.; Sawitzki, G.; Smith, C.; Smyth, G.; Tierney, L.; Yang, J. Y.; Zhang, J. *Genome Biol* **2004,** 5, (10), R80.
44. Oh, S.; Brammer, K. S.; Li, Y. S. J.; Teng, D.; Engler, A. J.; Chien, S.; Jin, S. *Proceedings of the National Academy of Sciences of the United States of America* **2009,** 106, (7), 2130-2135.
45. Park, J.; Bauer, S.; Schlegel, K. A.; Neukam, F. W.; von der Mark, K.; Schmuki, P. *Small* **2009,** 5, (6), 666-671.
46. Park, J.; Bauer, S.; Schmuki, P.; von der Mark, K. *Nano Lett* **2009**.
47. Park, J.; Bauer, S.; von der Mark, K.; Schmuki, P. *Nano Letters* **2007,** 7, (6), 1686-1691.
48. McLucas, E.; Moran, M. T.; Rochev, Y.; Carroll, W. M.; Smith, T. J. *Endothelium-Journal of Endothelial Cell Research* **2006,** 13, (1), 35-41.

49. Koster, R.; Vieluf, D.; Kiehn, M.; Sommerauer, M.; Kahler, J.; Baldus, S.; Meinertz, T.; Hamm, C. W. *Lancet* **2000,** 356, (9245), 1895-1897.
50. Jaalouk, D. E.; Lammerding, J. *Nature Reviews Molecular Cell Biology* **2009,** 10, (1), 63-73.
51. Chatzizisis, Y. S.; Coskun, A. U.; Jonas, M.; Edelman, E. R.; Feldman, C. L.; Stone, P. H. *Journal of the American College of Cardiology* **2007,** 49, (25), 2379-2393.
52. Tzima, E.; Del Pozo, M. A.; Kiosses, W. B.; Mohamed, S. A.; Li, S.; Chien, S.; Schwartz, M. A. *Embo Journal* **2002,** 21, (24), 6791-6800.
53. Iqbal, J.; Zaidi, M. *Biochemical and Biophysical Research Communications* **2005,** 328, (3), 751-755.
54. Kozian, D. H.; Ziche, M.; Augustin, H. G. *Lab Invest* **1997,** 76, (2), 267-76.
55. Phillips, D. J. *Domestic Animal Endocrinology* **2005,** 28, (1), 1-16.
56. Mccarthy, S. A.; Bicknell, R. *Journal of Biological Chemistry* **1993,** 268, (31), 23066-23071.
57. Klein, R.; Robertson, D. M.; Clarke, I. J. *Reproduction Fertility and Development* **1996,** 8, (2), 273-277.
58. Phillips, D. J.; Jones, K. L.; McGaw, D. J.; Groome, N. P.; Smolich, J. J.; Parsson, H.; de Kretser, D. M. *Journal of Clinical Endocrinology & Metabolism* **2000,** 85, (7), 2411-2415.
59. Jones, K. L.; de Kretser, D. M.; Phillips, D. J. *Journal of Endocrinology* **2004,** 181, (2), 307-314.
60. Perez, S.; Vial, E.; van Dam, H.; Castellazzi, M. *Oncogene* **2001,** 20, (9), 1135-1141.
61. Kawauchi, J.; Zhang, C.; Nobori, K.; Hashimoto, Y.; Adachi, M. T.; Noda, A.; Sunamori, M.; Kitajima, S. *Journal of Biological Chemistry* **2002,** 277, (41), 39025-39034.
62. Chiquet, M.; Gelman, L.; Lutz, R.; Maier, S. *Biochimica Et Biophysica Acta-Molecular Cell Research* **2009,** 1793, (5), 911-920.
63. Overholtzer, M.; Zhang, J.; Smolen, G. A.; Muir, B.; Li, W.; Sgroi, D. C.; Deng, C. X.; Brugge, J. S.; Haber, D. A. *Proceedings of the National Academy of Sciences of the United States of America* **2006,** 103, (33), 12405-12410.
64. Patel, V. P.; Kreider, B. L.; Li, Y.; Li, H.; Leung, K.; Salcedo, T.; Nardelli, B.; Pippalla, V.; Gentz, S.; Thotakura, R.; Parmelee, D.; Gentz, R.; Garotta, G. *J Exp Med* **1997,** 185, (7), 1163-72.
65. Youn, B. S.; Zhang, S. M.; Broxmeyer, H. E.; Cooper, S.; Antol, K.; Fraser, M., Jr.; Kwon, B. S. *Blood* **1998,** 91, (9), 3118-26.
66. Lebrin, F.; Goumans, M. J.; Jonker, L.; Carvalho, R. L. C.; Valdimarsdottir, G.; Thorikay, M.; Mummery, C.; Arthur, H. M.; ten Dijke, P. *Embo Journal* **2004,** 23, (20), 4018-4028.
67. Liu, Y. Q.; Jovanovic, B.; Pins, M.; Lee, C.; Bergan, R. C. *Oncogene* **2002,** 21, (54), 8272-8281.
68. Zhu, S.; Si, M. L.; Wu, H.; Mo, Y. Y. *J Biol Chem* **2007,** 282, (19), 14328-36.
69. Bryce, N. S.; Schevzov, G.; Ferguson, V.; Percival, J. M.; Lin, J. J.; Matsumura, F.; Bamburg, J. R.; Jeffrey, P. L.; Hardeman, E. C.; Gunning, P.; Weinberger, R. P. *Mol Biol Cell* **2003,** 14, (3), 1002-16.

70. Lian, Z.; Liu, J.; Li, L.; Li, X.; Tufan, N. L.; Wu, M. C.; Wang, H. Y.; Arbuthnot, P.; Kew, M.; Feitelson, M. A. *Mol Carcinog* **2004,** 40, (1), 34-46.
71. Spencer, J. A.; Hacker, S. L.; Davis, E. C.; Mecham, R. P.; Knutsen, R. H.; Li, D. Y.; Gerard, R. D.; Richardson, J. A.; Olson, E. N.; Yanagisawa, H. *Proc Natl Acad Sci U S A* **2005,** 102, (8), 2946-51.
72. Chiang, M. K.; Liao, Y. C.; Kuwabara, Y.; Lo, S. H. *Dev Biol* **2005,** 279, (2), 368-77.
73. Aerbajinai, W.; Lee, Y. T.; Wojda, U.; Barr, V. A.; Miller, J. L. *J Biol Chem* **2004,** 279, (3), 1916-21.
74. Ding, B.; Abe, J.; Wei, H.; Xu, H.; Che, W.; Aizawa, T.; Liu, W.; Molina, C. A.; Sadoshima, J.; Blaxall, B. C.; Berk, B. C.; Yan, C. *Proc Natl Acad Sci U S A* **2005,** 102, (41), 14771-6.
75. Fujioka, Y.; Taira, T.; Maeda, Y.; Tanaka, S.; Nishihara, H.; Iguchi-Ariga, S. M.; Nagashima, K.; Ariga, H. *J Biol Chem* **2001,** 276, (48), 45137-44.
76. Pandey, A.; Ozaki, K.; Baumann, H.; Levin, S. D.; Puel, A.; Farr, A. G.; Ziegler, S. F.; Leonard, W. J.; Lodish, H. F. *Nat Immunol* **2000,** 1, (1), 59-64.
77. Zhou, B.; Comeau, M. R.; De Smedt, T.; Liggitt, H. D.; Dahl, M. E.; Lewis, D. B.; Gyarmati, D.; Aye, T.; Campbell, D. J.; Ziegler, S. F. *Nat Immunol* **2005,** 6, (10), 1047-53.
78. Brown, V. I.; Hulitt, J.; Fish, J.; Sheen, C.; Bruno, M.; Xu, Q.; Carroll, M.; Fang, J.; Teachey, D.; Grupp, S. A. *Cancer Res* **2007,** 67, (20), 9963-70.
79. Benini, S.; Perbal, B.; Zambelli, D.; Colombo, M. P.; Manara, M. C.; Serra, M.; Parenza, M.; Martinez, V.; Picci, P.; Scotlandi, K. *Oncogene* **2005,** 24, (27), 4349-61.
80. Sawai, N.; Koike, K.; Mwamtemi, H. H.; Kinoshita, T.; Kurokawa, Y.; Sakashita, K.; Higuchi, T.; Takeuchi, K.; Shiohara, M.; Kamijo, T.; Ito, S.; Kato, T.; Miyazaki, H.; Yamashita, T.; Komiyama, A. *Blood* **1999,** 93, (11), 3703-12.
81. Landuzzi, L.; De Giovanni, C.; Nicoletti, G.; Rossi, I.; Ricci, C.; Astolfi, A.; Scopece, L.; Scotlandi, K.; Serra, M.; Bagnara, G. P.; Nanni, P.; Lollini, P. L. *Am J Pathol* **2000,** 157, (6), 2123-31.
82. Sawada, J.; Shimizu, S.; Tamatani, T.; Kanegasaki, S.; Saito, H.; Tanaka, A.; Kambe, N.; Nakahata, T.; Matsuda, H. *J Immunol* **2005,** 174, (6), 3626-32.
83. Xu, Y.; Zhu, K.; Hong, G.; Wu, W.; Baudhuin, L. M.; Xiao, Y.; Damron, D. S. *Nat Cell Biol* **2000,** 2, (5), 261-7.
84. Moody, T. W.; Zia, F.; Draoui, M.; Brenneman, D. E.; Fridkin, M.; Davidson, A.; Gozes, I. *Proc Natl Acad Sci U S A* **1993,** 90, (10), 4345-9.
85. Arita, Y.; Kihara, S.; Ouchi, N.; Maeda, K.; Kuriyama, H.; Okamoto, Y.; Kumada, M.; Hotta, K.; Nishida, M.; Takahashi, M.; Nakamura, T.; Shimomura, I.; Muraguchi, M.; Ohmoto, Y.; Funahashi, T.; Matsuzawa, Y. *Circulation* **2002,** 105, (24), 2893-8.
86. Ouchi, N.; Kobayashi, H.; Kihara, S.; Kumada, M.; Sato, K.; Inoue, T.; Funahashi, T.; Walsh, K. *J Biol Chem* **2004,** 279, (2), 1304-9.
87. Chandrasekar, B.; Boylston, W. H.; Venkatachalam, K.; Webster, N. J.; Prabhu, S. D.; Valente, A. J. *J Biol Chem* **2008,** 283, (36), 24889-98.
88. Loike, J. D.; Cao, L.; Budhu, S.; Hoffman, S.; Silverstein, S. C. *J Immunol* **2001,** 166, (12), 7534-42.

89. Scaffidi, A. K.; Petrovic, N.; Moodley, Y. P.; Fogel-Petrovic, M.; Kroeger, K. M.; Seeber, R. M.; Eidne, K. A.; Thompson, P. J.; Knight, D. A. *J Biol Chem* **2004,** 279, (36), 37726-33.
90. Lee, R. W.; Creed, T. J.; Schewitz, L. P.; Newcomb, P. V.; Nicholson, L. B.; Dick, A. D.; Dayan, C. M. *J Immunol* **2007,** 179, (11), 7941-8.
91. Baron, V.; De Gregorio, G.; Krones-Herzig, A.; Virolle, T.; Calogero, A.; Urcis, R.; Mercola, D. *Oncogene* **2003,** 22, (27), 4194-204.
92. Weisz, L.; Zalcenstein, A.; Stambolsky, P.; Cohen, Y.; Goldfinger, N.; Oren, M.; Rotter, V. *Cancer Res* **2004,** 64, (22), 8318-27.
93. Perez, S.; Vial, E.; van Dam, H.; Castellazzi, M. *Oncogene* **2001,** 20, (9), 1135-41.
94. Kawauchi, J.; Zhang, C.; Nobori, K.; Hashimoto, Y.; Adachi, M. T.; Noda, A.; Sunamori, M.; Kitajima, S. *J Biol Chem* **2002,** 277, (41), 39025-34.
95. Demeule, M.; Bertrand, Y.; Michaud-Levesque, J.; Jodoin, J.; Rolland, Y.; Gabathuler, R.; Beliveau, R. *Blood* **2003,** 102, (5), 1723-31.
96. Salcedo, R.; Young, H. A.; Ponce, M. L.; Ward, J. M.; Kleinman, H. K.; Murphy, W. J.; Oppenheim, J. J. *J Immunol* **2001,** 166, (12), 7571-8.
97. Woltmann, G.; McNulty, C. A.; Dewson, G.; Symon, F. A.; Wardlaw, A. J. *Blood* **2000,** 95, (10), 3146-52.
98. Lum, H.; Qiao, J.; Walter, R. J.; Huang, F.; Subbaiah, P. V.; Kim, K. S.; Holian, O. *Am J Physiol Heart Circ Physiol* **2003,** 285, (4), H1786-9.
99. Huang, F.; Mehta, D.; Predescu, S.; Kim, K. S.; Lum, H. *Endothelium* **2007,** 14, (1), 25-34.
100. Pierrot, C.; Beniguel, L.; Begue, A.; Khalife, J. *Biochem Biophys Res Commun* **2001,** 287, (4), 969-76.
101. Zhou, C.; Qiu, Y.; Pereira, F. A.; Crair, M. C.; Tsai, S. Y.; Tsai, M. J. *Neuron* **1999,** 24, (4), 847-59.
102. Mattson, M. P. *Antioxid Redox Signal* **2006,** 8, (11-12), 1997-2006.
103. Davis, M. C.; McColl, K. S.; Zhong, F.; Wang, Z.; Malone, M. H.; Distelhorst, C. W. *J Biol Chem* **2008,** 283, (16), 10357-65.
104. MacKeigan, J. P.; Murphy, L. O.; Blenis, J. *Nat Cell Biol* **2005,** 7, (6), 591-600.
105. Delpire, E.; Mount, D. B. *Annu Rev Physiol* **2002,** 64, 803-43.
106. Schubert, A.; Grimm, S. *Cancer Res* **2004,** 64, (1), 85-93.
107. Hall, C.; Nelson, D. M.; Ye, X.; Baker, K.; DeCaprio, J. A.; Seeholzer, S.; Lipinski, M.; Adams, P. D. *Mol Cell Biol* **2001,** 21, (5), 1854-65.
108. Cao, X.; Pfaff, S. L.; Gage, F. H. *Genes Dev* **2008,** 22, (23), 3320-34.
109. Overholtzer, M.; Zhang, J.; Smolen, G. A.; Muir, B.; Li, W.; Sgroi, D. C.; Deng, C. X.; Brugge, J. S.; Haber, D. A. *Proc Natl Acad Sci U S A* **2006,** 103, (33), 12405-10.
110. Schaffer, B. S.; Lin, M. F.; Byrd, J. C.; Park, J. H.; MacDonald, R. G. *Endocrinology* **2003,** 144, (3), 955-66.
111. Souza, R. F.; Wang, S.; Thakar, M.; Smolinski, K. N.; Yin, J.; Zou, T. T.; Kong, D.; Abraham, J. M.; Toretsky, J. A.; Meltzer, S. J. *Oncogene* **1999,** 18, (28), 4063-8.
112. Bennett, M.; Macdonald, K.; Chan, S. W.; Luzio, J. P.; Simari, R.; Weissberg, P. *Science* **1998,** 282, (5387), 290-3.
113. Osborn, S. L.; Sohn, S. J.; Winoto, A. *J Biol Chem* **2007,** 282, (31), 22786-92.

114. Yogosawa, S.; Hatakeyama, S.; Nakayama, K. I.; Miyoshi, H.; Kohsaka, S.; Akazawa, C. *J Biol Chem* **2005,** 280, (50), 41619-27.
115. Fortschegger, K.; Wagner, B.; Voglauer, R.; Katinger, H.; Sibilia, M.; Grillari, J. *Mol Cell Biol* **2007,** 27, (8), 3123-30.
116. Di Marcotullio, L.; Ferretti, E.; De Smaele, E.; Argenti, B.; Mincione, C.; Zazzeroni, F.; Gallo, R.; Masuelli, L.; Napolitano, M.; Maroder, M.; Modesti, A.; Giangaspero, F.; Screpanti, I.; Alesse, E.; Gulino, A. *Proc Natl Acad Sci U S A* **2004,** 101, (29), 10833-8.
117. Claude, A.; Zhao, B. P.; Kuziemsky, C. E.; Dahan, S.; Berger, S. J.; Yan, J. P.; Armold, A. D.; Sullivan, E. M.; Melancon, P. *J Cell Biol* **1999,** 146, (1), 71-84.
118. Gho, J. W.; Ip, W. K.; Chan, K. Y.; Law, P. T.; Lai, P. B.; Wong, N. *Cancer Res* **2008,** 68, (16), 6743-51.
119. Persengiev, S. P.; Devireddy, L. R.; Green, M. R. *Genes Dev* **2002,** 16, (14), 1806-14.
120. Aichberger, K. J.; Mayerhofer, M.; Gleixner, K. V.; Krauth, M. T.; Gruze, A.; Pickl, W. F.; Wacheck, V.; Selzer, E.; Mullauer, L.; Agis, H.; Sillaber, C.; Valent, P. *Blood* **2007,** 109, (7), 3031-41.
121. Adams, K. W.; Cooper, G. M. *J Biol Chem* **2007,** 282, (9), 6192-200.
122. Duckers, H. J.; Boehm, M.; True, A. L.; Yet, S. F.; San, H.; Park, J. L.; Clinton Webb, R.; Lee, M. E.; Nabel, G. J.; Nabel, E. G. *Nat Med* **2001,** 7, (6), 693-8.
123. Liu, X. M.; Peyton, K. J.; Ensenat, D.; Wang, H.; Schafer, A. I.; Alam, J.; Durante, W. *J Biol Chem* **2005,** 280, (2), 872-7.
124. Perrotti, D.; Iervolino, A.; Cesi, V.; Cirinna, M.; Lombardini, S.; Grassilli, E.; Bonatti, S.; Claudio, P. P.; Calabretta, B. *Mol Cell Biol* **2000,** 20, (16), 6159-69.
125. Hicks, G. G.; Singh, N.; Nashabi, A.; Mai, S.; Bozek, G.; Klewes, L.; Arapovic, D.; White, E. K.; Koury, M. J.; Oltz, E. M.; Van Kaer, L.; Ruley, H. E. *Nat Genet* **2000,** 24, (2), 175-9.
126. Koo, B. H.; Kim, D. S. *J Biol Chem* **2003,** 278, (52), 52578-86.
127. Toyoda, H.; Komurasaki, T.; Uchida, D.; Takayama, Y.; Isobe, T.; Okuyama, T.; Hanada, K. *J Biol Chem* **1995,** 270, (13), 7495-500.
128. Hao, Y.; Wong, R.; Feig, L. A. *Mol Cell Biol* **2008,** 28, (9), 2851-9.
129. Ryu, C. H.; Kim, S. W.; Lee, K. H.; Lee, J. Y.; Kim, H.; Lee, W. K.; Choi, B. H.; Lim, Y.; Kim, Y. H.; Hwang, T. K.; Jun, T. Y.; Rha, H. K. *Oncogene* **2005,** 24, (34), 5355-64.
130. Duchene, J.; Schanstra, J. P.; Pecher, C.; Pizard, A.; Susini, C.; Esteve, J. P.; Bascands, J. L.; Girolami, J. P. *J Biol Chem* **2002,** 277, (43), 40375-83.
131. Kakoki, M.; McGarrah, R. W.; Kim, H. S.; Smithies, O. *Proc Natl Acad Sci U S A* **2007,** 104, (18), 7576-81.
132. Berteaux, N.; Lottin, S.; Monte, D.; Pinte, S.; Quatannens, B.; Coll, J.; Hondermarck, H.; Curgy, J. J.; Dugimont, T.; Adriaenssens, E. *J Biol Chem* **2005,** 280, (33), 29625-36.
133. Castro, D. S.; Hermanson, E.; Joseph, B.; Wallen, A.; Aarnisalo, P.; Heller, A.; Perlmann, T. *J Biol Chem* **2001,** 276, (46), 43277-84.
134. Wallen, A.; Zetterstrom, R. H.; Solomin, L.; Arvidsson, M.; Olson, L.; Perlmann, T. *Exp Cell Res* **1999,** 253, (2), 737-46.

135. Moniwa, N.; Agata, J.; Hagiwara, M.; Ura, N.; Shimamoto, K. *Biol Chem* **2006,** 387, (2), 203-9.
136. Duchene, J.; Lecomte, F.; Ahmed, S.; Cayla, C.; Pesquero, J.; Bader, M.; Perretti, M.; Ahluwalia, A. *J Immunol* **2007,** 179, (7), 4849-56.
137. Komada, M.; Soriano, P. *Genes Dev* **1999,** 13, (11), 1475-85.
138. Wang, J.; Xiao, S. H.; Manley, J. L. *Genes Dev* **1998,** 12, (14), 2222-33.
139. Pires, N. M.; Pols, T. W.; de Vries, M. R.; van Tiel, C. M.; Bonta, P. I.; Vos, M.; Arkenbout, E. K.; Pannekoek, H.; Jukema, J. W.; Quax, P. H.; de Vries, C. J. *Circulation* **2007,** 115, (4), 493-500.
140. Oster, S. K.; Ho, C. S.; Soucie, E. L.; Penn, L. Z. *Adv Cancer Res* **2002,** 84, 81-154.
141. Haxsen, V.; Adam-Stitah, S.; Ritz, E.; Wagner, J. *Circ Res* **2001,** 88, (6), 637-44.
142. Kastner, P.; Messaddeq, N.; Mark, M.; Wendling, O.; Grondona, J. M.; Ward, S.; Ghyselinck, N.; Chambon, P. *Development* **1997,** 124, (23), 4749-58.
143. Toth, R.; Szegezdi, E.; Reichert, U.; Bernardon, J. M.; Michel, S.; Ancian, P.; Kis-Toth, K.; Macsari, Z.; Fesus, L.; Szondy, Z. *Eur J Immunol* **2001,** 31, (5), 1382-91.
144. Hiragun, T.; Peng, Z.; Beaven, M. A. *J Immunol* **2006,** 177, (4), 2047-50.
145. Dragone, L. L.; Myers, M. D.; White, C.; Sosinowski, T.; Weiss, A. *J Immunol* **2006,** 176, (1), 335-45.
146. Singla, D. K.; Sun, B. *Biochem Biophys Res Commun* **2005,** 332, (1), 135-41.
147. Ikedo, H.; Tamaki, K.; Ueda, S.; Kato, S.; Fujii, M.; Ten Dijke, P.; Okuda, S. *Int J Mol Med* **2003,** 11, (5), 645-50.
148. Bishay, K.; Ory, K.; Lebeau, J.; Levalois, C.; Olivier, M. F.; Chevillard, S. *Oncogene* **2000,** 19, (7), 916-23.
149. Deng, S.; Hirschberg, A.; Worzfeld, T.; Penachioni, J. Y.; Korostylev, A.; Swiercz, J. M.; Vodrazka, P.; Mauti, O.; Stoeckli, E. T.; Tamagnone, L.; Offermanns, S.; Kuner, R. *J Neurosci* **2007,** 27, (23), 6333-47.
150. Nicholson, A. C.; Hajjar, D. P. *Clin Chim Acta* **1999,** 286, (1-2), 23-9.
151. Ahmad, S. S.; Scandura, J. M.; Walsh, P. N. *J Biol Chem* **2000,** 275, (17), 13071-81.
152. Saxena, A.; Rorie, C. J.; Dimitrova, D.; Daniely, Y.; Borowiec, J. A. *Oncogene* **2006,** 25, (55), 7274-88.
153. Girnita, L.; Shenoy, S. K.; Sehat, B.; Vasilcanu, R.; Vasilcanu, D.; Girnita, A.; Lefkowitz, R. J.; Larsson, O. *J Biol Chem* **2007,** 282, (15), 11329-38.
154. Ge, L.; Shenoy, S. K.; Lefkowitz, R. J.; DeFea, K. *J Biol Chem* **2004,** 279, (53), 55419-24.
155. Van Eynde, A.; Nuytten, M.; Dewerchin, M.; Schoonjans, L.; Keppens, S.; Beullens, M.; Moons, L.; Carmeliet, P.; Stalmans, W.; Bollen, M. *Mol Cell Biol* **2004,** 24, (13), 5863-74.
156. Guo, D.; Hu, K.; Lei, Y.; Wang, Y.; Ma, T.; He, D. *J Biol Chem* **2004,** 279, (51), 53498-505.
157. Ohtsubo, M.; Kai, R.; Furuno, N.; Sekiguchi, T.; Sekiguchi, M.; Hayashida, H.; Kuma, K.; Miyata, T.; Fukushige, S.; Murotsu, T.; et al. *Genes Dev* **1987,** 1, (6), 585-93.
158. Chen, D.; Xu, W.; Bales, E.; Colmenares, C.; Conacci-Sorrell, M.; Ishii, S.; Stavnezer, E.; Campisi, J.; Fisher, D. E.; Ben-Ze'ev, A.; Medrano, E. E. *Cancer Res* **2003,** 63, (20), 6626-34.

159. Berk, M.; Desai, S. Y.; Heyman, H. C.; Colmenares, C. *Genes Dev* **1997,** 11, (16), 2029-39.
160. Henriet, P.; Zhong, Z. D.; Brooks, P. C.; Weinberg, K. I.; DeClerck, Y. A. *Proc Natl Acad Sci U S A* **2000,** 97, (18), 10026-31.
161. Rossi, D. J.; Londesborough, A.; Korsisaari, N.; Pihlak, A.; Lehtonen, E.; Henkemeyer, M.; Makela, T. P. *EMBO J* **2001,** 20, (11), 2844-56.
162. Trencia, A.; Perfetti, A.; Cassese, A.; Vigliotta, G.; Miele, C.; Oriente, F.; Santopietro, S.; Giacco, F.; Condorelli, G.; Formisano, P.; Beguinot, F. *Mol Cell Biol* **2003,** 23, (13), 4511-21.
163. Sakamoto, S.; Yokoyama, M.; Zhang, X.; Prakash, K.; Nagao, K.; Hatanaka, T.; Getzenberg, R. H.; Kakehi, Y. *Endocrinology* **2004,** 145, (6), 2929-40.
164. Kim, J.; Lee, K.; Pelletier, J. *Oncogene* **1998,** 16, (15), 1973-9.
165. Li, L.; Deng, B.; Xing, G.; Teng, Y.; Tian, C.; Cheng, X.; Yin, X.; Yang, J.; Gao, X.; Zhu, Y.; Sun, Q.; Zhang, L.; Yang, X.; He, F. *Proc Natl Acad Sci U S A* **2007,** 104, (19), 7951-6.
166. Yan, C.; Martinez-Quiles, N.; Eden, S.; Shibata, T.; Takeshima, F.; Shinkura, R.; Fujiwara, Y.; Bronson, R.; Snapper, S. B.; Kirschner, M. W.; Geha, R.; Rosen, F. S.; Alt, F. W. *EMBO J* **2003,** 22, (14), 3602-12.
167. Miyata, K.; Oike, Y.; Hoshii, T.; Maekawa, H.; Ogawa, H.; Suda, T.; Araki, K.; Yamamura, K. *Biochem Biophys Res Commun* **2005,** 329, (1), 296-304.
168. Zhao, H.; Ito, A.; Sakai, N.; Matsuzawa, Y.; Yamashita, S.; Nojima, H. *Circ J* **2006,** 70, (5), 615-24.
169. Teng, Y.; Zeisberg, M.; Kalluri, R. *J Clin Invest* **2007,** 117, (2), 304-6.
170. Niwa, Y.; Kanda, H.; Shikauchi, Y.; Saiura, A.; Matsubara, K.; Kitagawa, T.; Yamamoto, J.; Kubo, T.; Yoshikawa, H. *Oncogene* **2005,** 24, (42), 6406-17.
171. Yasukawa, H.; Hoshijima, M.; Gu, Y.; Nakamura, T.; Pradervand, S.; Hanada, T.; Hanakawa, Y.; Yoshimura, A.; Ross, J., Jr.; Chien, K. R. *J Clin Invest* **2001,** 108, (10), 1459-67.
172. Loughran, G.; Healy, N. C.; Kiely, P. A.; Huigsloot, M.; Kedersha, N. L.; O'Connor, R. *Mol Biol Cell* **2005,** 16, (4), 1811-22.
173. Bennett, R. D.; Mauer, A. S.; Strehler, E. E. *J Biol Chem* **2007,** 282, (5), 3205-12.
174. Sincock, P. M.; Fitter, S.; Parton, R. G.; Berndt, M. C.; Gamble, J. R.; Ashman, L. K. *J Cell Sci* **1999,** 112 (Pt 6), 833-44.
175. Itano, N.; Atsumi, F.; Sawai, T.; Yamada, Y.; Miyaishi, O.; Senga, T.; Hamaguchi, M.; Kimata, K. *Proc Natl Acad Sci U S A* **2002,** 99, (6), 3609-14.
176. Heckman, B. M.; Chakravarty, G.; Vargo-Gogola, T.; Gonzales-Rimbau, M.; Hadsell, D. L.; Lee, A. V.; Settleman, J.; Rosen, J. M. *Dev Biol* **2007,** 309, (1), 137-49.
177. McCormick, C.; Duncan, G.; Goutsos, K. T.; Tufaro, F. *Proc Natl Acad Sci U S A* **2000,** 97, (2), 668-73.
178. Fehrenbacher, N.; Bastholm, L.; Kirkegaard-Sorensen, T.; Rafn, B.; Bottzauw, T.; Nielsen, C.; Weber, E.; Shirasawa, S.; Kallunki, T.; Jaattela, M. *Cancer Res* **2008,** 68, (16), 6623-33.
179. Prasad, D. V.; Parekh, V. V.; Joshi, B. N.; Banerjee, P. P.; Parab, P. B.; Chattopadhyay, S.; Kumar, A.; Mishra, G. C. *J Immunol* **2002,** 169, (4), 1801-9.

180. Chauhan, A. K.; Motto, D. G.; Lamb, C. B.; Bergmeier, W.; Dockal, M.; Plaimauer, B.; Scheiflinger, F.; Ginsburg, D.; Wagner, D. D. *J Exp Med* **2006,** 203, (3), 767-76.
181. Kim, Y. S.; Kang, H. S.; Herbert, R.; Beak, J. Y.; Collins, J. B.; Grissom, S. F.; Jetten, A. M. *Mol Cell Biol* **2008,** 28, (7), 2358-67.
182. Nanda, N.; Bao, M.; Lin, H.; Clauser, K.; Komuves, L.; Quertermous, T.; Conley, P. B.; Phillips, D. R.; Hart, M. J. *J Biol Chem* **2005,** 280, (26), 24680-9.
183. Duke-Cohan, J. S.; Gu, J.; McLaughlin, D. F.; Xu, Y.; Freeman, G. J.; Schlossman, S. F. *Proc Natl Acad Sci U S A* **1998,** 95, (19), 11336-41.
184. Li, X.; Tu, L.; Murphy, P. G.; Kadono, T.; Steeber, D. A.; Tedder, T. F. *J Leukoc Biol* **2001,** 69, (4), 565-74.
185. Gomez-Cambronero, J.; Horn, J.; Paul, C. C.; Baumann, M. A. *J Immunol* **2003,** 171, (12), 6846-55.
186. Lee, T. C.; Ho, I. C.; Lu, W. J.; Huang, J. D. *J Biol Chem* **2006,** 281, (27), 18401-7.
187. Li, Z.; Shi, H. Y.; Zhang, M. *Oncogene* **2005,** 24, (12), 2008-19.
188. Tadros, A.; Hughes, D. P.; Dunmore, B. J.; Brindle, N. P. *Blood* **2003,** 102, (13), 4407-9.
189. Borrell-Pages, M.; Canals, J. M.; Cordelieres, F. P.; Parker, J. A.; Pineda, J. R.; Grange, G.; Bryson, E. A.; Guillermier, M.; Hirsch, E.; Hantraye, P.; Cheetham, M. E.; Neri, C.; Alberch, J.; Brouillet, E.; Saudou, F.; Humbert, S. *J Clin Invest* **2006,** 116, (5), 1410-24.
190. Lin, K. R.; Lee, S. F.; Hung, C. M.; Li, C. L.; Yang-Yen, H. F.; Yen, J. J. *J Biol Chem* **2007,** 282, (30), 21962-72.
191. Nakano, K.; Vousden, K. H. *Mol Cell* **2001,** 7, (3), 683-94.
192. Liu, L.; Sakai, T.; Sano, N.; Fukui, K. *Biochem J* **2004,** 380, (Pt 1), 31-41.
193. Kaminker, P. G.; Kim, S. H.; Taylor, R. D.; Zebarjadian, Y.; Funk, W. D.; Morin, G. B.; Yaswen, P.; Campisi, J. *J Biol Chem* **2001,** 276, (38), 35891-9.
194. Albayrak, T.; Scherhammer, V.; Schoenfeld, N.; Braziulis, E.; Mund, T.; Bauer, M. K.; Scheffler, I. E.; Grimm, S. *Mol Biol Cell* **2003,** 14, (8), 3082-96.

CHAPTER 7: Supplemental Information

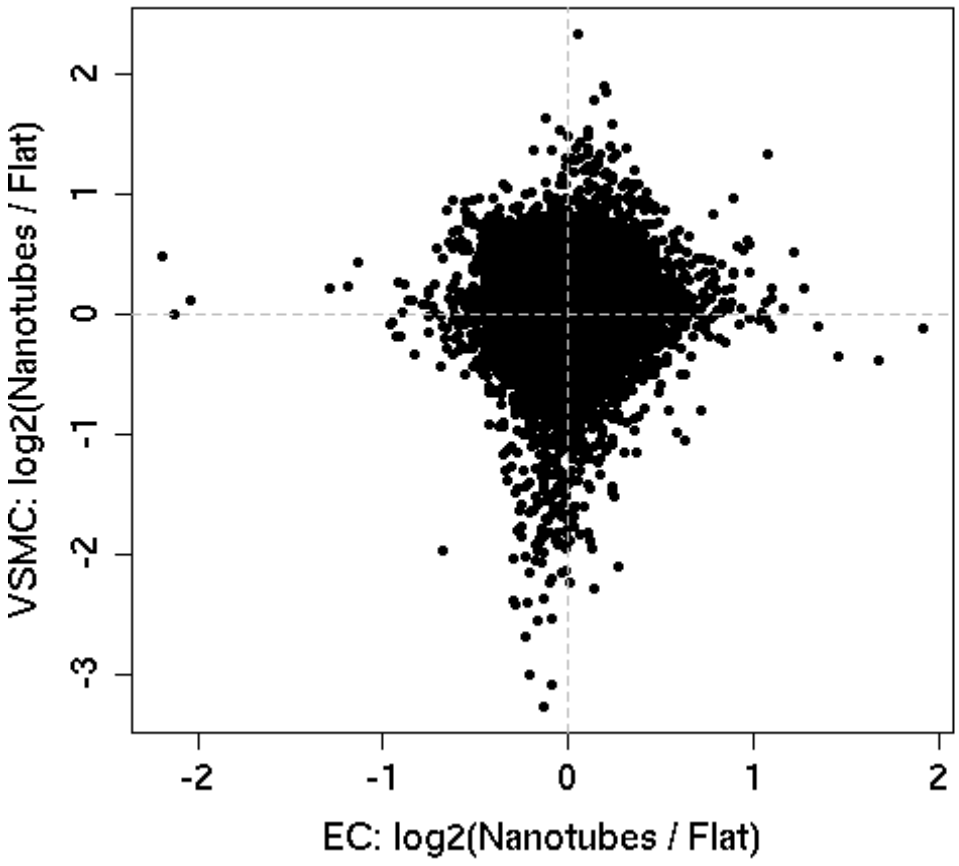

Figure S1: MM plot of gene expression for VSMCs vs. ECs.

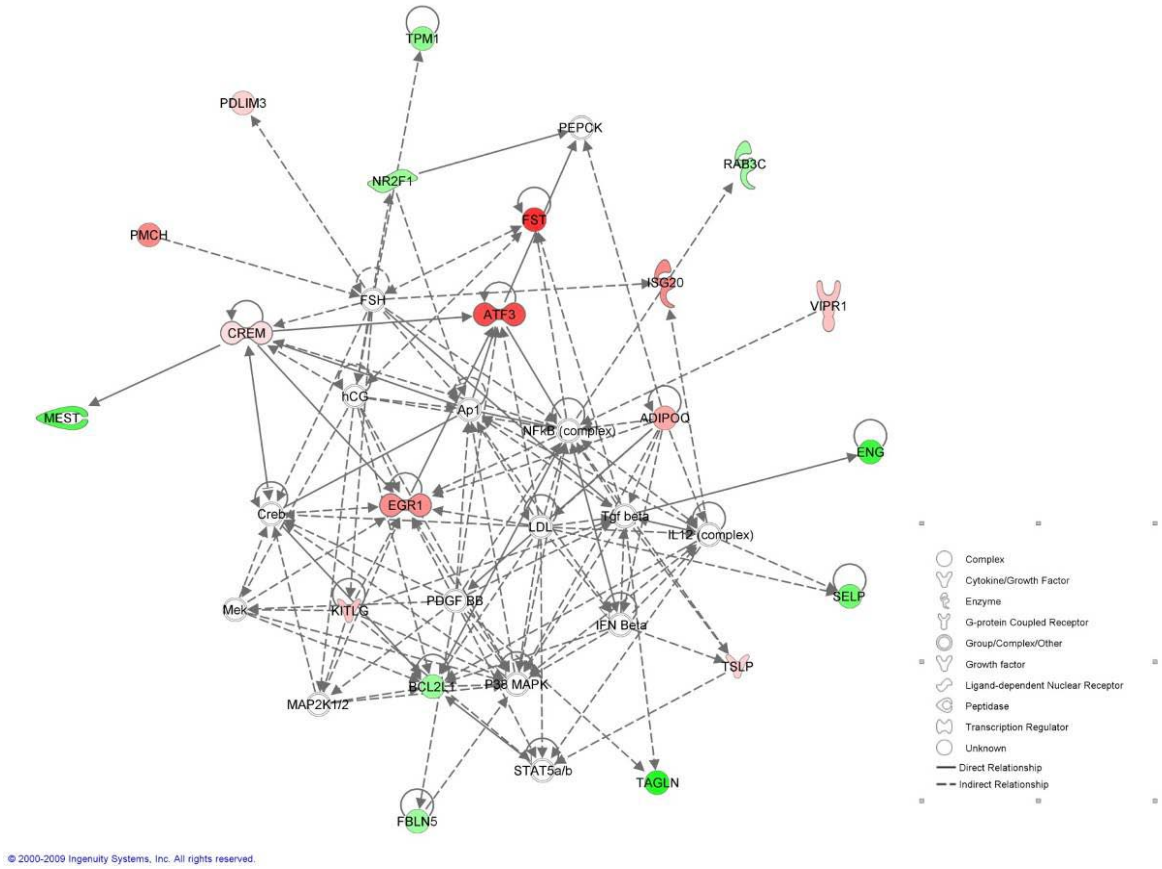

Figure S2. Original top network plot for ECs generated by Ingenuity Pathway Analysis. Red indicates upregulation, green down regulation. Intensity of color is proportional to magnitude of change.

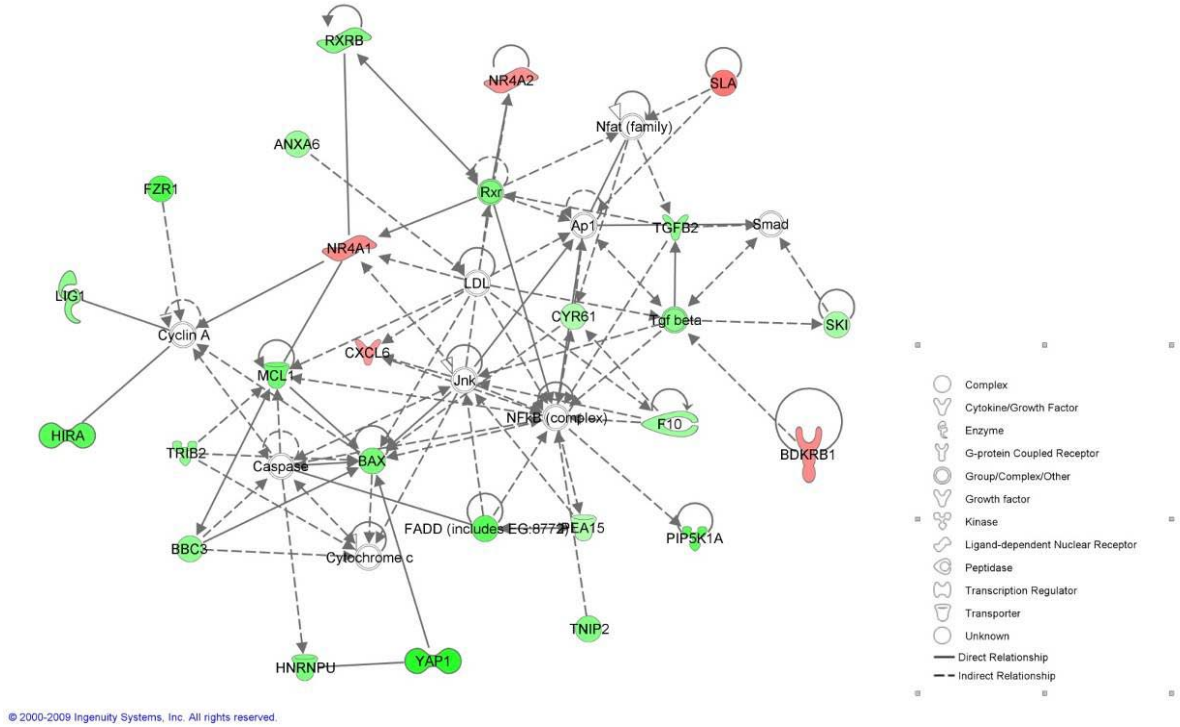

Figure S3. Original top network plot for VSMCs generated by Ingenuity Pathway Analysis. Red indicates upregulation, green down regulation. Intensity of color is proportional to magnitude of change.

Table S1: Genes significantly affected by exposure to nanotubes are listed according to their affect on a specific process. Those that have been shown in literature to inhibit a process are listed on the left two columns, and those that promote the process are listed on the right columns. Superscript refers to literature identified through IPA's curated findings that support all of the gene's classification(s). Data from these tables were used to plot Figures 1B and 4B.

A. Human Aortic Endothelial Cells

Proliferation/Cell Cycle Progression

Inhibit	log2FC.NTvsTi	Promote	log2FC.NTvsTi
CCL23[64, 65]	-0.84	ENG[66, 67]	-0.83
TPM1[68, 69]	-0.47	RPS15A[70]	-0.33
FBLN5[71]	-0.41	TNS3[72]	0.34
CAPRIN2[73]	-0.19	CREM[74]	0.3
PFDN5[75]	-0.32	TSLP[76-78]	0.43
NOV[79]	0.6	KITLG[80-82]	0.54
GPR68[83]	0.63	VIPR1[84]	0.56
ADIPOQ[85-87]	0.8	TNXB[88, 89]	0.55
		ISG20[90]	1.1
		EGR1[91, 92]	1.04
		ATF3[93, 94]	1.67
		FST[54]	1.91

Migration

Inhibit	log2FC.NTvsTi	Promote	log2FC.NTvsTi
ENG[66, 67]	-0.83	TPM1[68, 69]	-0.47
		FBLN5[71]	-0.41
		KITLG[80-82]	0.54
		MFI2[95]	0.6
		NOV[79]	0.6
		ADIPOQ[85-87]	0.8
		CCR3[96]	1.03
		FST[54]	1.91

Inflammation/Coagulation

Inhibit	log2FC.NTvsTi	Promote	log2FC.NTvsTi
KITLG[80-82]	0.54	CCL23[64, 65]	-0.84
TNXB[88, 89]	0.55	SELP[97]	-0.61
		GPR4[98, 99]	-0.49
		IL13RA1[100]	-0.34
		TSLP[76-78]	0.43

Apoptosis/Cell Death

Inhibit	log2FC.NTvsTi	Promote	log2FC.NTvsTi
NR2F1[101]	-0.42	CAPRIN2[73]	-0.19
GPX3[102]	0.34	ITPR3[103]	0.44
TSLP[76-78]	0.43	CREM[74]	0.3

NEK8[104]	0.67		
ADIPOQ[85-87]	0.8		
SLC12A2[105]	0.72		
PPID[96, 106]	0.84		
EGR1[91, 92]	1.04		
ATF3[93, 94]	1.67		

B. Human Aortic Vascular Smooth Muscle Cells

Proliferation/Cell Cycle Progression

Inhibit	log2FC.NTvsTi	Promote	log2FC.NTvsTi
HIRA[107]	-2.4	YAP1[108, 109]	-3.09
IGF2R[110, 111]	-1.83	FADD[112, 113]	-2.38
VPS18[114]	-1.6	PRPF19[115]	-2.15
KCTD11[116]	-1.43	GBF1[117]	-2.13
ATF5[118, 119]	-1.36	MCL1[120, 121]	-2.07
HMOX1[122, 123]	-1.06	FUS[124, 125]	-2.04
EREG[126, 127]	1.02	RALGDS[128, 129]	-2.02
BDKRB2[130, 131]	1.17	H19[132]	-1.92
NR4A2[133, 134]	1.22	IGF2R[110, 111]	-1.83
BDKRB1[131, 135, 136]	1.3	SFRS5[137,138]	-1.82
NR4A1[139, 140]	1.33	RXRB[141-143]	-1.81
SLA[144, 145]	1.53	TGFB2[146, 147]	-1.67
		LIG1[148]	-1.61

		SEMA4C[149]	-1.56
		F10[150, 151]	-1.42
		NCL[152]	-1.42
		ARRB1[153, 154]	-1.32
		PPP1R8[155]	-1.26
		THG1L[156]	-1.26
		RCC1[157]	-1.25
		SKI[158, 159]	-1.25
		ITGA2[160]	-1.2
		PEA15[161, 162]	-1.12
		CYR61[163]	-1.12
		EWSR1[164]	-1.1
		RBBP6[165]	-1.08
		WASF2[166]	-1.02
		EREG[126, 127]	1.02

Migration

Inhibit	log2FC.NTvsTi	Promote	log2FC.NTvsTi
ABHD2[167]	-1.95	PRKAG1[86]	-2.69
TMBIM1[168]	-1.21	HNRPAB[169]	-2.15
SOCS3[170, 171]	-1.01	SEMA4C[149]	-1.56
		ARRB1[153, 154]	-1.32
		PDLIM2[172]	-1.23
		ITGA2[160]	-1.2
		WASF2[166]	-1.02
		MYO10[173]	-1.01
		CD151[174]	-1
		BDKRB1[131, 135, 136]	1.29
		HAS1[175]	1.36
		IRS2[176]	2.32

Inflammation/Coagulation

Inhibit	log2FC.NTvsTi	Promote	log2FC.NTvsTi
EXT1[177]	-1.16	LAMP1[178, 179]	-2.23
ADAMTS13[180]	1.2	RALGDS[128, 129]	-2.02
GLIS2[181]	1.52	PEAR1[182]	-1.8
SLA[144, 145]	1.53	ATRN[183]	-1.63
		CHST2[184]	-1.58
		F10[150, 151]	-1.42
		CXCL6[185]	1.16
		BDKRB1[131, 135,	1.3

Apoptosis/Cell Death

Inhibit	log2FC.NTvsTi	Promote	log2FC.NTvsTi
YAP1[108, 109]	-3.09	FADD[112, 113]	-2.38
PRPF19[115]	-2.15	LAMP1[178, 179]	-2.23
MCL1[120, 121]	-2.07	AQP3[186]	-2.1
SFRS5[137, 138]	-1.82	FUS[124, 125]	-2.04
RXRB[141-143]	-1.81	BAX[187]	-1.92
TNIP2[188]	-1.81	IGF2R[110, 111]	-1.83
DNAJB2[189]	-1.72	TRIB2[190]	-1.67
ATF5[118, 119]	-1.36	BBC3[191]	-1.61
THG1L[156]	-1.26	UACA[192]	-1.49
SKI[158, 159]	-1.25	NCL[152]	-1.42
PEA15[161, 162]	-1.12	TNKS2[193]	-1.31
RBBP6[165]	-1.08	SDHC[194]	-1.17
HMOX1	-1.06	SOCS3[170, 171]	-1.01
BDKRB2[130, 131]	1.17	NR4A1[139, 140]	1.33
NR4A2[133, 134]	1.22		

BDKRB1[131, 135, 136]	1.29		
IRS2[176]	2.32		

Publishing Agreement

It is the policy of the University to encourage the distribution of all theses, dissertations, and manuscripts. Copies of all UCSF theses, dissertations, and manuscripts will be routed to the library via the Graduate Division. The library will make all theses, dissertations, and manuscripts accessible to the public and will preserve these to the best of their abilities, in perpetuity.

Please sign the following statement:

I hereby grant permission to the Graduate Division of the University of California, San Francisco to release copies of my thesis, dissertation, or manuscript to the Campus Library to provide access and preservation, in whole or in part, in perpetuity.

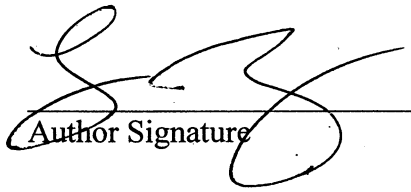

Author Signature

3/17/2010

Date